Ltd., Japan, REC-RCAB0002PF) in a humid chamber. Slides were washed in wash buffer (3x) and incubated with goat anti-rabbit secondary antibody, AlexaFluor488-conjugated (1:500 in blocking buffer; 45 min; Invitrogen) in a humid chamber. Slides were washed once with wash buffer and once in PBS and mounted in Vectashield containing DAPI. Cells were scored visually on a Leica DM IRBE epifluorescence microscope equipped with a 100x PL APO 1.40 oil objective. Images were collected sequentially on a confocal laser scanning microscope (Leica TCS SP5; 63x Plan APO 1.4 oil objective, NA 1.4, Milton Keynes, UK), equipped with a 405 diode and an Argon (488 nm) laser, and pinhole equivalent to 1 Airy disk. For comparison of Nanog staining during Ring1B depletion, images were collected on the same day using the same settings, and without saturation of the intensity signal. Raw TIFF images were merged in Adobe Photoshop (Adobe Systems, Edinburgh, UK) without further thresholding or filtering (*e.g.* no background subtraction).

Supplementary References

1. Billon, N., Jolicoeur, C., Ying, Q. L., Smith, A. & Raff, M. Normal timing of oligodendrocyte development from genetically engineered, lineage-selectable mouse ES cells. *J. Cell Sci.* **115**, 3657-3665 (2002).
2. Niwa, H., Miyazaki, J. & Smith, A. G. Quantitative expression of Oct-3/4 defines differentiation, dedifferentiation or self-renewal of ES cells. *Nat. Genet.* **24**, 372-376 (2000).
3. Mak, W. *et al.* Mitotically stable association of polycomb group proteins eed and enx1 with the inactive X chromosome in trophoblast stem cells. *Curr. Biol.* **12**, 1016-1020 (2002).
4. Kunath, T. *et al.* Imprinted X-inactivation in extra-embryonic endoderm cell lines from mouse blastocysts. *Development* **132**, 1649-1661 (2005).
5. Szutorisz, H. *et al.* Formation of an active tissue-specific chromatin domain initiated by epigenetic marking at the embryonic stem cell stage. *Mol. Cell. Biol.* **25**, 1804-1820 (2005).
6. Azuara, V. *et al.* Chromatin signatures of pluripotent cell lines. *Nat. Cell Biol.* **8**, 532-538 (2006).
7. Daniel, T. & Carling, D. Functional analysis of mutations in the gamma 2 subunit of AMP-activated protein kinase associated with cardiac hypertrophy and Wolff-Parkinson-White syndrome. *J. Biol. Chem.* **277**, 51017-51024 (2002).
8. de Napoles, M. *et al.* Polycomb group proteins Ring1A/B link ubiquitylation of histone H2A to heritable gene silencing and X inactivation. *Dev. Cell* **7**, 663-676 (2004).
9. Kuzmichev, A., Nishioka, K., Erdjument-Bromage, H., Tempst, P. & Reinberg, D. Histone methyltransferase activity associated with a human multiprotein complex containing the Enhancer of Zeste protein. *Genes Dev.* **16**, 2893-2905 (2002).
10. Atsuta, T. *et al.* Production of monoclonal antibodies against mammalian Ring1B proteins. *Hybridoma* **20**, 43-46 (2001).
11. Chao, S. H. & Price, D. H. Flavopiridol inactivates P-TEFb and blocks most RNA polymerase II transcription in vivo. *J. Biol. Chem.* **276**, 31793-31799 (2001).
12. Lam, L. T. *et al.* Genomic-scale measurement of mRNA turnover and the mechanisms of action of the anti-cancer drug flavopiridol. *Genome Biol.* **2**, RESEARCH0041 (2001).
13. Arceci, R. J., King, A. A., Simon, M. C., Orkin, S. H. & Wilson, D. B. Mouse GATA-4: a retinoic acid-inducible GATA-binding transcription factor expressed in endodermally derived tissues and heart. *Mol Cell Biol* **13**, 2235-2246 (1993).
14. Singh, A. M., Hamazaki, T., Hankowski, K. E. & Terada, N. A Heterogeneous Expression Pattern for Nanog in Embryonic Stem Cells. *Stem Cells* 25, 2534-2542 (2007).
15. Bernstein, B. E. *et al.* A bivalent chromatin structure marks key developmental genes in embryonic stem cells. *Cell* **125**, 315-326 (2006).

LETTERS

The SRA protein Np95 mediates epigenetic inheritance by recruiting Dnmt1 to methylated DNA

Jafar Sharif[1,2,3]*, Masahiro Muto[4]*, Shin-ichiro Takebayashi[6]*, Isao Suetake[7], Akihiro Iwamatsu[8], Takaho A. Endo[5], Jun Shinga[4], Yoko Mizutani-Koseki[4], Tetsuro Toyoda[5], Kunihiro Okamura[2], Shoji Tajima[7], Kohzoh Mitsuya[1], Masaki Okano[6] & Haruhiko Koseki[4]

DNA methyltransferase (cytosine-5) 1 (Dnmt1) is the principal enzyme responsible for maintenance of CpG methylation and is essential for the regulation of gene expression, silencing of parasitic DNA elements, genomic imprinting and embryogenesis[1–4]. Dnmt1 is needed in S phase to methylate newly replicated CpGs occurring opposite methylated ones on the mother strand of the DNA, which is essential for the epigenetic inheritance of methylation patterns in the genome. Despite an intrinsic affinity of Dnmt1 for such hemi-methylated DNA[5], the molecular mechanisms that ensure the correct loading of Dnmt1 onto newly replicated DNA *in vivo* are not understood. The Np95 (also known as Uhrf1 and ICBP90) protein binds methylated CpG through its SET and RING finger-associated (SRA) domain[6]. Here we show that localization of mouse Np95 to replicating heterochromatin is dependent on the presence of hemi-methylated DNA. Np95 forms complexes with Dnmt1 and mediates the loading of Dnmt1 to replicating heterochromatic regions. By using Np95-deficient embryonic stem cells and embryos, we show that Np95 is essential *in vivo* to maintain global and local DNA methylation and to repress transcription of retrotransposons and imprinted genes. The link between hemi-methylated DNA, Np95 and Dnmt1 thus establishes key steps of the mechanism for epigenetic inheritance of DNA methylation.

Methylation inheritance is the process of copying pre-existing methylation patterns onto the new DNA strand after DNA replication[7]. Dnmt1 prefers to methylate hemi-methylated CpG regions, which appear after the replication and repair steps, and thus has a dominant role in methylation inheritance[8]. Loading of Dnmt1 onto its targets involves proliferating cell nuclear antigen (Pcna), which promotes Dnmt1 localization to replication foci, but Pcna is not absolutely required in this process[9,10]. Therefore, the molecular mechanisms that load Dnmt1 to the hemi-methylated CpG regions remain largely obscure. Recently, the *Arabidopsis* SRA protein VIM1 has been shown to be involved in recognition of methylated CpG and DNA methylation[11]. A closely related human protein NP95 also binds to methylated promoters through its SRA domain, and mouse Np95 is essential for cell-cycle progression, DNA damage responses and replication of pericentromeric heterochromatin[6,12–14]. Therefore, Np95 is a possible candidate linking Dnmt1 with hemi-methylated DNA in mammals.

To test this possibility, we first examined the localization of Np95 in embryonic stem cells (ESCs) by immunofluorescence analysis. Because Np95 is known to colocalize with replication foci in mid-to-late-S-phase fibroblasts[14], we sorted ESCs into representative cell-cycle stages and then stained them with 4,6-diamidino-2-phenylindole (DAPI), and Np95, Dnmt1 and Pcna antibodies (Fig. 1a). There was an intense accumulation of Np95 at DAPI-dense heterochromatin regions in mid-to-late-S-phase nuclei, but not in the G1 or G2/M phase. We confirmed colocalization of Np95 with Dnmt1 and Pcna in mid-to-late-S-phase ESC nuclei, an observation that prompted us to investigate whether human NP95 forms complexes with DNMT1. *In vivo* biotinylated NP95 was used in a pull-down assay[15] (Supplementary Fig. 1). We tested for the presence of DNMT1 in NP95 complexes by immunoblotting, and found significant quantities (Fig. 1b) of catalytically active NP95-associated DNMT1 (ref. 16, Supplementary Fig. 2). Because DNMT1 interacts with PCNA[9,10], we extended the analysis to PCNA and also found PCNA in the NP95 complexes (Fig. 1b). Taken together, these results indicate that NP95 forms complexes with DNMT1 and PCNA at replicating heterochromatic regions[17], where hemi-methylated DNA is generated and concurrently converted into full-methylated DNA on both strands.

We next examined whether the localization of Np95 is dependent on methylated DNA using various *Dnmt*-deficient ESCs with characteristic DNA methylation profiles. In wild-type ESCs, Np95 exhibited a focal accumulation in replicated heterochromatin in a small fraction of cells (~20%) and a diffuse localization pattern in the rest (Fig. 1c–e). A similar Np95 distribution profile was seen in *Dnmt3a*$^{-/-}$;*Dnmt3b*$^{-/-}$ double-knockout (DKO) ESCs (Fig. 1c–e), which retain considerable global DNA methylation[18]. Np95 was also able to localize to heterochromatin in *Dnmt1*$^{-/-}$ ESCs (Fig. 1c, e), in which global DNA methylation is extensively decreased but not abolished[18,19]. Interestingly, the percentage of *Dnmt1*$^{-/-}$ ESCs showing Np95 heterochromatin accumulation was much higher than in wild-type and 3abDKO ESCs (Fig. 1c). In contrast, Np95 showed a diffuse localization pattern and almost no enrichment in the newly replicated heterochromatin in *Dnmt1*$^{-/-}$;*Dnmt3a*$^{-/-}$;*Dnmt3b*$^{-/-}$ triple knockout (TKO) ESCs (Fig. 1c–e), in which DNA methylation is absent[19]. These findings support the idea that localization of Np95 to replicating heterochromatin is dependent on methylated DNA. To confirm this, we transiently expressed Dnmt3a and Dnmt3b, both of which methylate DNA at pericentric heterochromatin, as either wild-type or catalytically defective mutants in TKO ESCs and examined the heterochromatin localization of Np95 (refs 20 and 21; Fig. 1f and Supplementary Fig. 3). Dnmt3a and Dnmt3b restored the heterochromatin localization of Np95, whereas the catalytically defective mutants did not. These findings indicate that the heterochromatin

[1]Tohoku University Biomedical Engineering Research Organization (TUBERO), 2-1 Seiryo-machi, Aoba-ku, Sendai 980-8575, Japan. [2]Department of Obstetrics and Gynecology, Tohoku University School of Medicine, 1-1 Seiryo-machi, Aoba-ku, Sendai 980-8574, Japan. [3]Department of Chemistry and Biotechnology, Graduate School of Engineering, The University of Tokyo, 7-3-1 Hongo, Bunkyo-ku, Tokyo 113-8656, Japan. [4]RIKEN Research Center for Allergy and Immunology, [5]RIKEN Genomic Sciences Center, 1-7-22 Suehiro, Tsurumi-ku, Yokohama 230-0045, Japan. [6]RIKEN Center for Developmental Biology, 2-2-3 Minatojima-minamimachi, Chuo-ku, Kobe, Hyogo 650-0047, Japan. [7]Institute for Protein Research, Osaka University, 3-2 Yamadaoka, Suita, Osaka 565-0871, Japan. [8]Protein-Research Network, Inc., 1-13-5 Fukuura, Kanazawa-ku, Yokohama 236-0004, Japan.
*These authors contributed equally to this work.

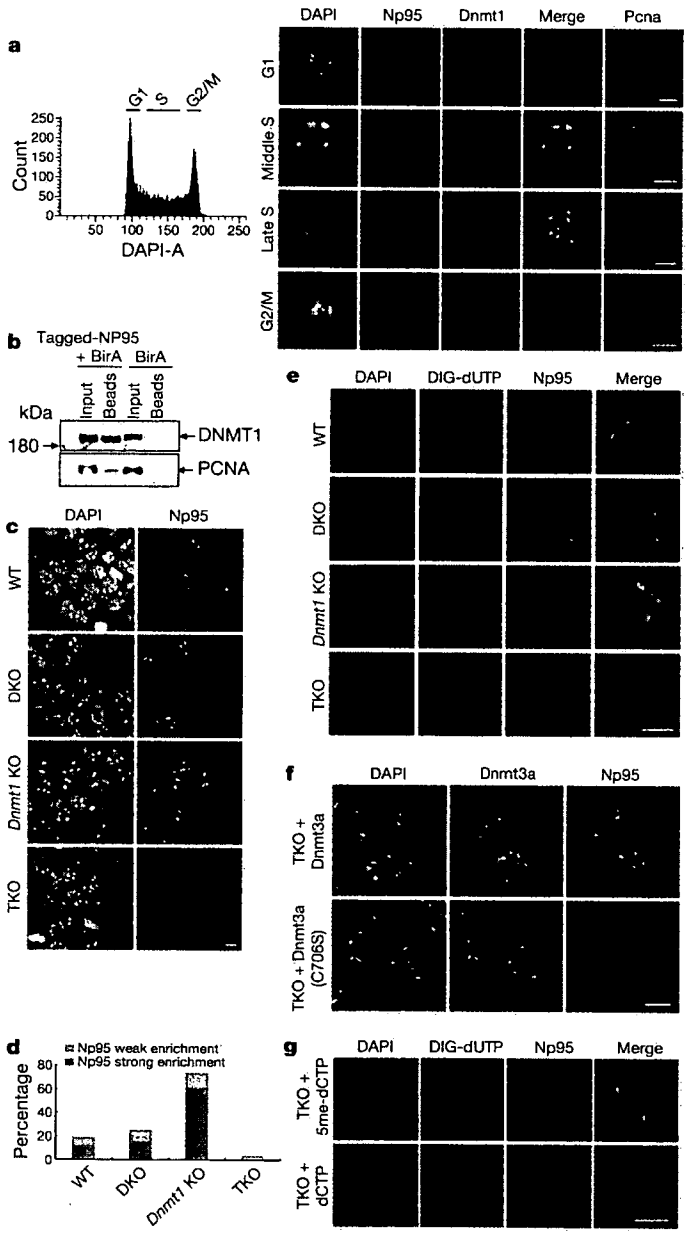

Figure 1 | Local accumulation of Np95 is dependent on hemi-methylated DNA. **a**, Representative subnuclear localization of Np95, Dnmt1 and Pcna in wild-type (WT) ESCs (E14) during cell-cycle progression (right). Merged images for Np95 and Dnmt1 are shown. Profile of DNA content in exponentially growing ESCs is shown (left). DAPI-A is an arbitrary unit that represents fluorescent intensity of cells stained by DAPI. **b**, Association of NP95 with DNMT1 and PCNA in HeLa cell nuclear extracts. HeLa cells transfected with expression vectors for BirA *Escherichia coli* biotin-protein ligase and tagged-NP95 are indicated as 'Tagged-NP95 + BirA', whereas those transfected with BirA alone are labelled 'BirA'. **c**, Immunofluorescence analysis of Np95 in wild-type, *Dnmt3a*$^{-/-}$;*Dnmt3b*$^{-/-}$ DKO, *Dnmt1* knockout (KO) and *Dnmt1*$^{-/-}$;*Dnmt3a*$^{-/-}$;*Dnmt3b*$^{-/-}$ TKO ESCs. **d**, Frequency of cells exhibiting heterochromatic localization of Np95 in respective ESCs. More than three-hundred cells were visually scored for the degree of speckled localization of Np95 for either strong or weak enrichment at the heterochromatic regions. **e**, Nuclear localization of Np95 during replication of the pericentromeric heterochromatin. Replication sites were visualized by the incorporation of digoxigenin-11 (DIG)-dUTP. **f**, Localization of Np95 in TKO ESCs, in which a wild-type or catalytic-defective (C706S) Dnmt3a was transiently expressed. **g**, Localization of Np95 in TKO ESCs, in which methylated or unmethylated dCTP was incorporated simultaneously with DIG-dUTP. Scale bars represent 10 μm.

accumulation of Np95 during S phase is dependent on the DNA methylation mark rather than on the presence of Dnmt3 proteins.

Given that the primary Dnmt1 substrate for methylation inheritance is hemi-methylated DNA, we hypothesized that Np95 primarily recognizes hemi-methylated CpG, which is enriched in newly replicated regions and thus is distributed in the nuclei in a cell-cycle-dependent manner. Consistent with this hypothesis, Np95 accumulated in heterochromatin in most *Dnmt1*$^{-/-}$ ESCs independently of the cell-cycle stage, whereas the heterochromatin enrichment of Np95 was barely detectable in the early S phase of the wild-type cells (Fig. 1c and Supplementary Fig. 4). This difference could be explained by increased hemi-methylated CpG in *Dnmt1*$^{-/-}$ ESCs, as has been seen in *DNMT1*-defective human cancer cells[22], whereas heterochromatic regions are probably symmetrically CpG-methylated in wild-type ESCs in early S phase. We thus examined colocalization of Np95 and hemi-methylated DNA by replication labelling, in which 5-methyl-dCTP is incorporated into the nascent strand of an unmethylated TKO genome[23]. Np95 was prominently accumulated in heterochromatin when 5-methyl-dCTP was incorporated into TKO ESCs (Fig. 1g). These results strongly support a model in which local accumulation of Np95 is dependent on hemi-methylated DNA. Consistent with our observations, the recombinant SRA domain has been shown recently to bind hemi-methylated CpG *in vitro*[24].

We went on to examine the affect of Np95 loss on DNA methylaion[13] (Supplementary Fig. 5). *Np95*$^{-/-}$ embryos show developmental arrest shortly after gastrulation and exhibit early gestational lethality in a similar manner to *Dnmt1*$^{-/-}$ embryos. Genomic DNA isolated from *Np95*$^{-/-}$ and wild-type ESCs or embryos was evaluated for the degree of global and local DNA methylation. *Dnmt1*$^{-/-}$ ESCs were used as a reference in these experiments[18]. The level of global DNA methylation in the absence of Np95 was determined by examining the resistance of the DNA to methylation-sensitive restriction enzymes. Global CpG methylation was reduced substantially in *Np95*$^{-/-}$ ESCs and embryos (Fig. 2a).

To refine our analysis, we next examined CpG methylation levels at heterochromatic domains. Major and minor satellites at pericentromeric and centromeric heterochromatin, respectively, are highly compacted and condensed; this is, at least in part, caused by the high levels of methylated CpG. DNA blot analyses for major and minor satellites revealed extensive hypomethylation in both *Np95*$^{-/-}$ and *Dnmt1*$^{-/-}$ ESCs (Fig. 2b). We further investigated CpG methylation levels by immuofluorescence using a 5-methylcytosine antibody. Intense 5-methylcytosine staining at pericentromeric regions was seen in the mitotic chromosomes and interphase nuclei of wild-type ESCs, but was significantly reduced in *Dnmt1*$^{-/-}$ and was totally abolished in TKO cells (Fig. 2c). In *Np95*$^{-/-}$ ESCs, 5-methylcytosine staining was reduced to a level similar to that in *Dnmt1*$^{-/-}$ ESCs, but was less than levels in TKO cells. The methylation defect in *Np95*$^{-/-}$ cells was complemented by expression of Myc-tagged Np95. Equivalent data were obtained for the major satellite sequences by DNA bot analyses (Supplementary Fig. 6). In summary, CpG methylation in heterochromatic regions is reduced to a similar extent in *Np95*$^{-/-}$ and *Dnmt1*$^{-/-}$ ESCs.

Most CpGs are methylated at retrotransposon-derived elements in euchromatic regions. Loss of DNA methylation by Dnmt1 inactivation results in derepression of silenced retrotransposons[4]. We thus examined DNA methylation at the promoter regions of the intracisternal A particle (IAP) and long interspersed nuclear element 1 (LINE-1) retrotransposons. Hypomethylation of IAP retrotransposons in *Np95*$^{-/-}$ ESCs was demonstrated by DNA blot analysis (Fig. 2d). Moreover, hypomethylation of IAP and LINE-1 elements in *Np95*$^{-/-}$ embryos was confirmed by bisulphite genomic sequencing (Fig. 2e). Prompted by these findings, we further investigated whether Np95 has a role in genomic imprinting, which is mediated by DNA methylation in somatic cells[2]. CpG methylation at the imprinting control regions of imprinted *H19*, *Kcnq1ot1* (also known as *Lit1*)

and *Gtl2* genes was reduced in *Np95*$^{-/-}$ ESCs (Fig. 2e). Taken together, these results implicate Np95 in DNA methylation at both heterochromatin and euchromatin compartments.

We went on to test whether defects in DNA methylation perturb transcriptional repression in *Np95*$^{-/-}$ embryos. Indeed, RNAi-mediated knockdown of Np95 has been reported to increase pericentromeric transcription[14]. Similarly, in our analysis, IAP, LINE-1 and short interspersed nuclear element 1 (SINE-1) retrotransposons were derepressed in *Np95*$^{-/-}$ embryos (Fig. 3a). We also examined whether parent-of-origin-specific expression at imprinted *H19* and *Kcnq1ot1* loci was retained in *Np95*$^{-/-}$ embryos. In the wild-type embryos, maternally derived *H19* and paternally derived *Kcnq1ot1* were exclusively expressed, whereas, in *Np95*$^{-/-}$ embryos, both alleles were expressed (Fig. 3b). This was accompanied by silencing of the adjacent imprinted transcripts within the clusters (*Igf2* and *Cdkn1c*). Therefore, Np95 is essential for transcriptional silencing of heterochromatin and retrotransposons as well as for parent-of-origin-specific expression of imprinted genes through regulation of CpG methylation status. Taken together, Dnmt1-dependent CpG methylation requires its association with Np95, indicating that Np95 is required either to stimulate the catalytic activity or to direct recruitment of Dnmt1 to its DNA targets.

To test the first possibility, we examined the expression and catalytic activity of Dnmt1 in the absence of Np95. Dnmt1 expression and catalytic activity were comparable in wild-type and *Np95*$^{-/-}$ ESCs (Fig. 4a). We also confirmed that expression of both Dnmt3a and Dnmt3b were maintained (Supplementary Fig. 7). We then addressed the second possibility by determining whether Np95 affects Dnmt1 subnuclear localization. Dnmt1 had either a diffuse localization pattern or a focal accumulation in heterochromatin in wild-type ESCs, as shown in previous studies[17], whereas in almost all *Np95*$^{-/-}$ ESCs Dnmt1 had a diffuse localization pattern (Fig. 4b). The wild-type phenotype was restored by introduction of Myc-tagged Np95. In wild-type cells, Dnmt1 accumulated in the replicating pericentromeric heterochromatin regions in mid-S-phase, and partially retained its heterochromatin localization in late S phase. In contrast, no significant enrichment of Dnmt1 in heterochromatin was observed throughout the S phase in *Np95*$^{-/-}$ ESCs (Fig. 4c). These results demonstrate the requirement of Np95 for proper localization of Dnmt1. Because subnuclear localization of Dnmt1 is dependent on pre-existing DNA methylation marks[23,25] and Np95 binds methylated CpG[24], Np95 is shown to link Dnmt1 to methylated DNA.

Our findings extend our understanding of the molecular mechanism that ensures the fidelity and efficacy of DNA methylation. We have identified binding of the SRA-domain protein Np95 to pre-existing methylated CpG, probably in a hemi-methylated state, as an essential process in loading Dnmt1 to hemi-methylated sites where it mediates accurate and sufficient DNA methylation after

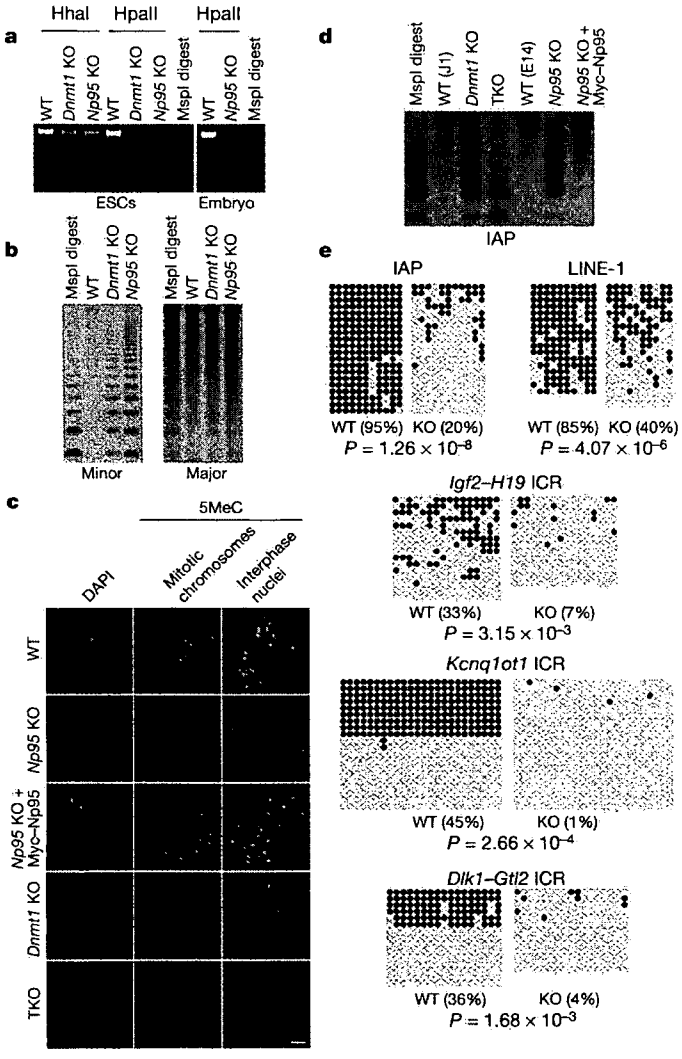

Figure 2 | Impairment of DNA methylation status on *Np95* gene inactivation. **a**, Genome-wide DNA demethylation in *Np95* KO ESCs (left) and embryos (right). **b**, DNA demethylation at the centromeric minor (left) and major (right) satellite repeats. **c**, Anti-5-methylcytosine (5MeC) immunofluorescence in wild-type (WT), *Np95* KO, *Np95* KO + Myc–Np95, *Dnmt1* KO and TKO ESCs in mitotic chromosomes and interphase nuclei. Scale bars represent 10 μm. **d**, DNA demethylation at the IAP retrotransposons. J1 and E14 cells are the parental ESCs for *Dnmt1* and *Np95* KO, respectively. **e**, Extensive demethylation of retrotransposons and imprinting centres in *Np95* KO embryos and ESCs, respectively. Bisulphite sequencing results obtained from E9.5 mouse embryos for IAP and LINE-1, and from ESCs for imprinting control regions (ICRs) of *Igf2–H19*, *Kcnq1ot1* and *Dlk–Gtl2*, are shown. The overall percentage of methylated CpGs is indicated in parentheses. The *P* values indicate the significance of the difference between wild-type and *Np95* KO embryos.

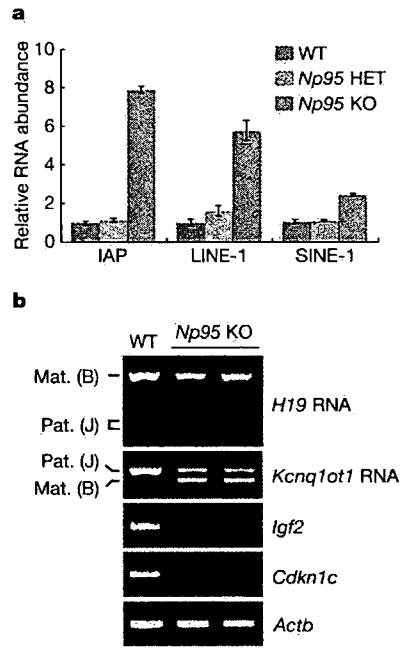

Figure 3 | Misexpression of hypomethylated genes on *Np95* gene inactivation. **a**, Transcriptional derepression of endogenous retrotransposons in *Np95* KO embryos. Error bars represent standard deviation. Total RNA derived from wild-type (WT), heterozygotes (HET) and KO embryos were used. **b**, Disruption of functional imprinting at the two imprinted gene clusters. Monoallelic expression of *H19* (paternal repression) and *Kcnq1ot1* (maternal repression) was lost completely, whereas expression of *Igf2* and *Cdkn1c* was absent in *Np95* KO embryos. B, C57BL/6 strain; J, JF1 strain; Mat., maternal; Pat., paternal; *Actb*, β-actin.

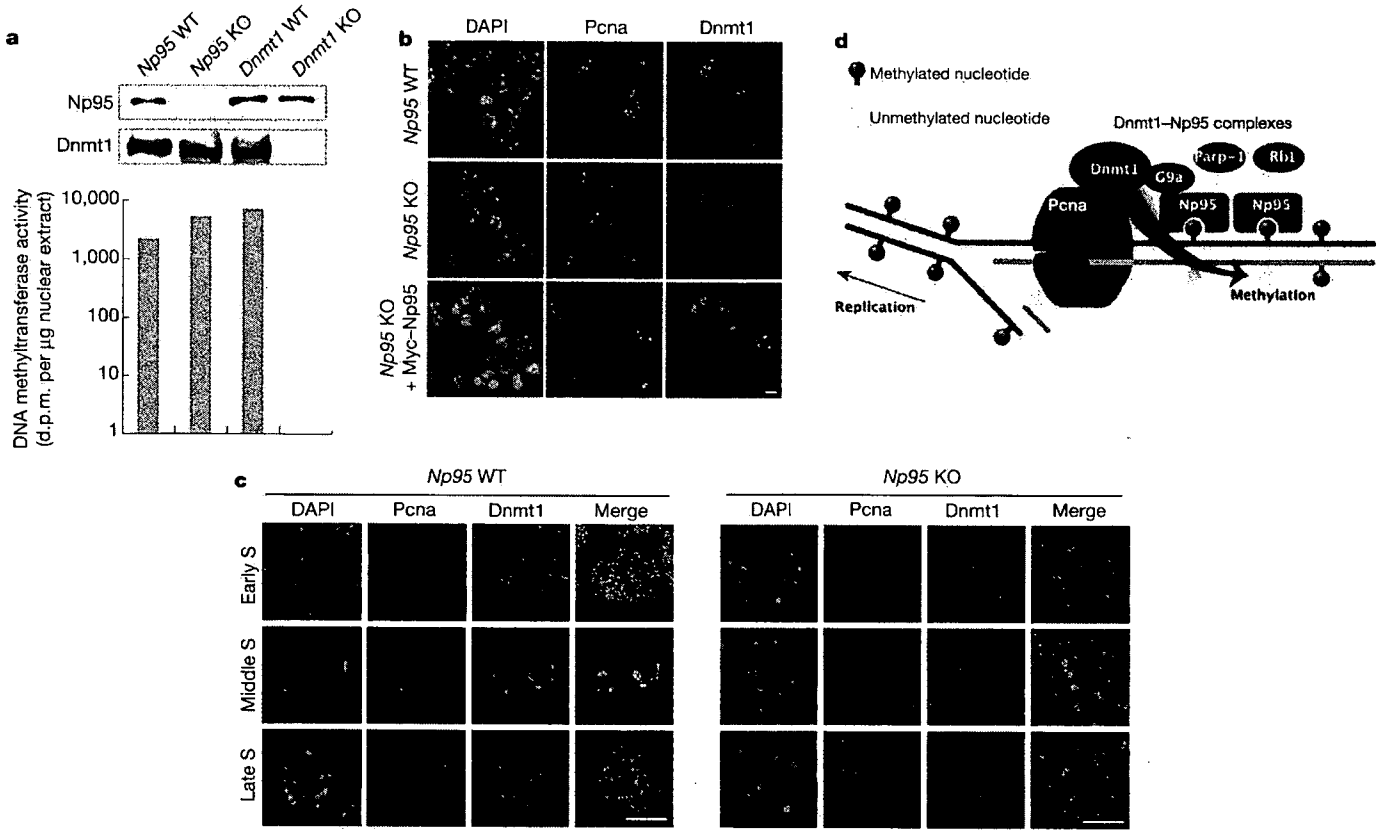

Figure 4 | Np95 is required to target Dnmt1. a, DNA methyltransferase activity and the expression of Dnmt1 in *Np95* KO ESCs. d.p.m., decay per minute. **b**, Immunofluorescence analysis of Dnmt1 and Pcna in wild-type, *Np95* KO, and *Np95* KO + Myc–Np95 ESCs. **c**, Nuclear localization of Dnmt1 (green) with Pcna (red) in the early S phase, middle S phase and late S phase of wild-type or *Np95* KO ESCs. The merged images at the right show overlays of Pcna and Dnmt1 staining. The relative contribution of the S-phase stage was not altered in *Np95* KO ESCs (Supplementary Fig. 8). **d**, Schematic representation of molecular actions of Dnmt1–Np95 complexes at the replicating heterochromatic regions identified in this study. Pre-existing and newly synthesized DNA strands are indicated by green and blue lines, respectively. Scale bars represent 10 μm.

replication (Fig. 4d). Consistent with this model, the Np95 SRA domain preferentially binds to hemi-methylated CpG dinucleotides[24]. It is noteworthy that Np95 forms complexes with nuclear proteins involved in DNA repair and chromatin modifications and/or functions[6,14] (Supplementary Tables 1 and 2). The role of Np95 in linking Dnmt1 with DNA repair is probably represented by hypersensitivity to DNA damage observed in the absence of Np95 (ref. 13). Moreover, Np95 complexes share Pcna, Rb1, Parp1 and G9a with Dnmt1 (refs 9 and 26–28; Fig. 1b and Supplementary Table 1). This suggests the involvement of Np95 in sensing not only CpG methylation status but also other chromatin features to guarantee appropriate localization of Dnmt1 (Fig. 4d). Intriguingly, similar methylation defects are seen in cells deficient in Cxxc1, an unmethylated CpG binding protein[29]. This suggests that more proteins recognize CpG methylation status in mediating levels of genomic methylation. Collectively, our findings provide the first evidence that the SRA-domain protein Np95 is required for a hallmark feature of the epigenome, the coordinate regulation of local and global epigenetic features.

METHODS SUMMARY

Immunofluorescence analysis. Detailed procedures for immunostaining and imaging are described in Methods. The following antibodies were used: Np95 rat monoclonal antibody[13], Dnmt1 rabbit polyclonal antibody (Santa Cruz Biotechnology, sc-20701), Pcna mouse monoclonal antibody (Santa Cruz Biotechnology, sc-56), Alexa Fluor-488 goat anti-mouse immunoglobulin G (Molecular Probes, A11017) and Alexa Fluor-555 goat anti-rabbit immunoglobulin G (Molecular Probes, A21430).

Replication labelling. Nucleotide analogues were introduced into cells by a hypotonic shift method as described previously[23,30], with slight modifications as described in Methods.

Pull down of NP95 complexes from HeLa cell extracts. *NP95* complementary DNA was amino-terminally tagged with an oligonucleotide encoding a 23-amino acid biotin-binding domain[15] and was subcloned into pCAGGS. Procedures for cell culture and protein purification are described in Methods.

Mice. *Np95*-deficient mice were generated by using R1 ESCs according to standard protocols, and backcrossed onto a C57BL/6 background for three to six generations[13]. Schematic representations of *Np95* genomic organization and its targeting strategy are illustrated in Supplementary Fig. 1.

DNA methylation analysis. The degree of DNA methylation was assessed by DNA blot hybridization, bisulphite genomic sequencing and 5-methylcytosine immunostaining as described in Methods. Results of bisulphite genomic sequencing were statistically examined as described in Methods.

RNA expression analysis. PCR with reverse transcription analysis was carried out as described in the Methods. Primers used in this study are listed in Supplementary Table 3. Detailed PCR conditions used in this work are available on request.

DNA methyltransferase activity. DNA methyltransferase activity was determined as described previously[16].

Full Methods and any associated references are available in the online version of the paper at www.nature.com/nature.

Received 27 July; accepted 22 October 2007.
Published online 11 November 2007.

1. Li, E., Bestor, T. H. & Jaenisch, R. Targeted mutation of the DNA methyltransferase gene results in embryonic lethality. *Cell* 69, 915–926 (1992).
2. Li, E., Beard, C. & Jaenisch, R. Role for DNA methylation in genomic imprinting. *Nature* 366, 362–365 (1993).
3. Jackson-Grusby, L. *et al.* Loss of genomic methylation causes p53-dependent apoptosis and epigenetic deregulation. *Nature Genet.* 27, 31–39 (2001).
4. Walsh, C. P., Chaillet, J. R. & Bestor, T. H. Transcription of IAP endogenous retroviruses is constrained by cytosine methylation. *Nature Genet.* 20, 116–117 (1998).

5. Fatemi, M., Hermann, A., Pradhan, S. & Jeltsch, A. The activity of the murine DNA methyltransferase Dnmt1 is controlled by interaction of the catalytic domain with the N-terminal part of the enzyme leading to an allosteric activation of the enzyme after binding to methylated DNA. *J. Mol. Biol.* **309**, 1189–1199 (2001).
6. Unoki, M., Nishidate, T. & Nakamura, Y. ICBP90, an E2F-1 target, recruits HDAC1 and binds to methyl-CpG through its SRA domain. *Oncogene* **23**, 7601–7610 (2004).
7. Klose, R. J. & Bird, A. P. Genomic DNA methylation: the mark and its mediators. *Trends Biochem. Sci.* **31**, 89–97 (2006).
8. Goll, M. G. & Bestor, T. H. Eukaryotic cytosine methyltransferases. *Annu. Rev. Biochem.* **74**, 481–514 (2005).
9. Chuang, L. S. *et al.* Human DNA-(cytosine-5) methyltransferase-PCNA complex as a target for p21WAF1. *Science* **277**, 1996–2000 (1997).
10. Spada, F. *et al.* DNMT1 but not its interaction with the replication machinery is required for maintenance of DNA methylation in human cells. *J. Cell Biol.* **176**, 565–571 (2007).
11. Woo, H. R., Pontes, O., Pikaard, C. S. & Richards, E. J. VIM1, a methylcytosine-binding protein required for centromeric heterochromatinization. *Genes Dev.* **21**, 267–277 (2007).
12. Bonapace, I. M. *et al.* Np95 is regulated by E1A during mitotic reactivation of terminally differentiated cells and is essential for S phase entry. *J. Cell Biol.* **157**, 909–914 (2002).
13. Muto, M. *et al.* Targeted disruption of *Np95* gene renders murine embryonic stem cells hypersensitive to DNA damaging agents and DNA replication blocks. *J. Biol. Chem.* **277**, 34549–34555 (2002).
14. Papait, R. *et al.* Np95 is implicated in pericentromeric heterochromatin replication and in major satellite silencing. *Mol. Biol. Cell* **18**, 1098–1106 (2007).
15. de Boer, E. *et al.* Efficient biotinylation and single-step purification of tagged transcription factors in mammalian cells and transgenic mice. *Proc. Natl Acad. Sci. USA* **100**, 7480–7485 (2003).
16. Suetake, I., Miyazaki, J., Murakami, C., Takeshima, H. & Tajima, S. Distinct enzymatic properties of recombinant mouse DNA methyltransferases Dnmt3a and Dnmt3b. *J. Biochem.* **133**, 737–744 (2003).
17. Leonhardt, H., Page, A. W., Weier, H. U. & Bestor, T. H. A targeting sequence directs DNA methyltransferase to sites of DNA replication in mammalian nuclei. *Cell* **71**, 865–873 (1992).
18. Okano, M., Bell, D. W., Haber, D. A. & Li, E. DNA methyltransferases Dnmt3a and Dnmt3b are essential for *de novo* methylation and mammalian development. *Cell* **99**, 247–257 (1999).
19. Tsumura, A. *et al.* Maintenance of self-renewal ability of mouse embryonic stem cells in the absence of DNA methyltransferases Dnmt1, Dnmt3a and Dnmt3b. *Genes Cells* **11**, 805–814 (2006).
20. Bachman, K. E., Rountree, M. R. & Baylin, S. B. Dnmt3a and Dnmt3b are transcriptional repressors that exhibit unique localization properties to heterochromatin. *J. Biol. Chem.* **276**, 32282–32287 (2001).
21. Lin, I. G. *et al.* Murine *de novo* methyltransferase Dnmt3a demonstrates strand asymmetry and site preference in the methylation of DNA *in vitro*. *Mol. Cell. Biol.* **22**, 704–723 (2002).
22. Chen, T. *et al.* Complete inactivation of DNMT1 leads to mitotic catastrophe in human cancer cells. *Nature Genet.* **39**, 391–396 (2007).
23. Takebayashi, S., Tamura, T., Matsuoka, C. & Okano, M. Major and essential role for DNA methylation mark in mouse embryogenesis and stable association of DNMT1 with newly replicated regions. *Mol. Cell. Biol.* **27**, 8243–8258 (2007).
24. Bostick, M. *et al.* UHRF1 plays a role in maintaining DNA methylation in mammalian cells. *Science* **317**, 1760–1764 (2007).
25. Damelin, M. & Bestor, T. H. Biological functions of DNA methyltransferase 1 require its methyltransferase activity. *Mol. Cell. Biol.* **27**, 3891–3899 (2007).
26. Pradhan, S. & Kim, G. D. The retinoblastoma gene product interacts with maintenance human DNA (cytosine-5) methyltransferase and modulates its activity. *EMBO J.* **21**, 779–788 (2002).
27. Reale, A. *et al.* Modulation of DNMT1 activity by ADP-ribose polymers. *Oncogene* **24**, 13–19 (2005).
28. Estève, P. O. *et al.* Direct interaction between DNMT1 and G9a coordinates DNA and histone methylation during replication. *Genes Dev.* **20**, 3089–3103 (2006).
29. Carlone, D. L. *et al.* Reduced genomic cytosine methylation and defective cellular differentiation in embryonic stem cells lacking CpG binding protein. *Mol. Cell. Biol.* **25**, 4881–4891 (2005).
30. Koberna, K. *et al.* Nuclear organization studied with the help of a hypotonic shift: its use permits hydrophilic molecules to enter into living cells. *Chromosoma* **108**, 325–335 (1999).

Supplementary Information is linked to the online version of the paper at www.nature.com/nature.

Acknowledgements This work was supported in part by a grant from the Genome Network Project (to H.K.), by the 'Ground-based Research Program for Space Utilization' promoted by the Japan Space Forum (H.K.) and by a grant-in-aid for Scientific Research on Priority Areas (germ-cell development, reprogramming and epigenetics, to M.O. and K.M.) from the Ministry of Education, Culture, Sports, Science and Technology, Japan. We thank W. Reik, N. Brockdorff, P. Burrows, H. Niwa, H. Sano, J. Strouboulis and M. Vidal for critical reading and reagents.

Author Contributions J. Sharif., K.O. and K.M. performed DNA methylation and gene expression analyses; M.M., Y.M.-K. and H.K. generated, maintained and performed phenotypic analyses of knockout mice; M.M., J. Shinga. and A.I. purified the protein complexes and performed mass spectrometry analyses; S. Takebayashi and M.O. performed immunofluorescence analysis; M.M., I.S. and S. Tajima performed the DNA methylation assay; and T.A.E. and T.T. performed statistical analyses. K.M., M.O. and H.K. designed the study, wrote the paper and contributed equally as co-senior authors. All authors discussed the results and commented on the manuscript.

Author Information Reprints and permissions information is available at www.nature.com/reprints. Correspondence and requests for materials should be addressed to H.K. (koseki@rcai.riken.jp).

MOLECULAR AND CELLULAR BIOLOGY, Jan. 2008, p. 293–301
0270-7306/08/$08.00+0 doi:10.1128/MCB.00473-07

Vol. 28, No. 1

Altered Quality Control in the Endoplasmic Reticulum Causes Cortical Dysplasia in Knock-In Mice Expressing a Mutant BiP▽

Naoya Mimura,[1,2] Shigeki Yuasa,[3] Miho Soma,[3] Hisayo Jin,[1] Keita Kimura,[2] Shigemasa Goto,[2] Haruhiko Koseki,[4] and Tomohiko Aoe[1]*

Department of Anesthesiology[1] and Department of Medicine and Clinical Oncology,[2] Chiba University Graduate School of Medicine, 1-8-1 Inohana, Chuo-ku, Chiba City, Chiba 260-8670, Department of Ultrastructural Research, National Institute of Neuroscience, National Center of Neurology and Psychiatry, 4-1-1 Ogawahigashi, Kodaira, Tokyo 187-8502,[3] and Laboratory for Developmental Genetics, RIKEN Research Center for Allergy and Immunology, 1-7-22 Suehiro, Tsurumi, Yokohama 230-0045,[4] Japan

Received 20 March 2007/Returned for modification 21 June 2007/Accepted 2 October 2007

Binding immunoglobulin protein (BiP) is an endoplasmic reticulum (ER) molecular chaperone that is central to ER function. We examined knock-in mice expressing a mutant BiP in order to elucidate physiological processes that are sensitive to BiP functions during development and adulthood. The mutant BiP lacked the retrieval sequence that normally functions to return BiP to the ER from the secretory pathway. This allowed us to examine the effects of a defect in ER function without completely eliminating BiP function. The homozygous mutant BiP neonates died after birth due to respiratory failure. Besides that, the mutant BiP mice displayed disordered layer formation in the cerebral cortex and cerebellum, a neurological phenotype of *reeler* mutant-like malformation. Consistent with the phenotype, Cajal-Retzius (CR) cells did not secrete reelin, and the expression of reelin was markedly reduced posttranscriptionally. Furthermore, the reduction in the size of the whole brain and the apparent scattering of CR cells throughout the cortex, which were distinct from the *reeler* phenotype, were also seen. These findings suggest that the maturation and secretion of reelin in CR cells and other factors related to neural migration may be sensitive to aberrant ER quality control, which may cause various neurological disorders.

Proteins destined for the secretory pathway are inserted into the endoplasmic reticulum (ER) cotranslationally and subjected to quality control (12, 25). Aberrant protein folding due to extracellular stimuli such as ischemia, hypoxia, and genetic mutations results in the accumulation of misfolded proteins in the ER, which causes ER stress and initiates the unfolded protein response (UPR) (35, 39) that enhances the capacity for ER quality control by reducing general protein synthesis (18), producing ER chaperones, and promoting ER-associated degradation (4, 6). A failure of this adaptation mechanism may cause cellular dysfunction and cell death, resulting in diverse human disorders (24, 26) such as neurodegenerative disease (21, 23), cardiomyopathy (15), and diabetes (17, 34). Furthermore, mutant mouse models have revealed that the UPR plays a vital role during normal development by increasing protein synthesis, as necessary, of dedicated secretory cells (46) such as pancreatic beta cells (38), plasma cells (37), hepatocytes (36), and alveolar type II epithelial cells (29). Inadequate adaptation to these physiological demands may lead to diverse diseases.

ER molecular chaperones and folding enzymes such as binding immunoglobulin protein (BiP), calnexin, and protein disulfide isomerase facilitate the correct folding or degradation of these newly synthesized proteins as well as of misfolded proteins. BiP, also called the 78-kDa glucose-regulated protein (GRP78), is a member of the heat shock protein 70 (HSP70) family of proteins and is one of the most abundant ER chaperones, assisting in protein translocation, folding, and degradation (31). ER chaperones localize to the ER by two mechanisms: retention and retrieval (40). BiP is retained in the ER by interacting with other ER proteins and the ER matrix. When misfolded proteins accumulate in the ER, BiP is secreted from the ER together with the misfolded proteins, where it assists with protein refolding, or it helps in the degradation of these proteins (16, 47). In post-ER compartments, the carboxyl-terminal Lys-Asp-Glu-Leu (KDEL) sequence of BiP is then recognized by the KDEL receptor, which facilitates the return of BiP to the ER (27, 30).

The complete depletion of BiP has lethal effects on mammalian early embryonic cells (28). *Saccharomyces cerevisiae* BiP (Kar2p) is essential for survival, while the deletion of the retrieval sequence (His-Asp-Glu-Leu [HDEL] in yeast) is dispensable because the UPR is activated, and the loss of the chaperone in the ER is compensated for (3). Therefore, to elucidate physiological processes that are sensitive to BiP functions during development and adulthood in multicellular organisms, we produced knock-in mice expressing a mutant BiP in which the retrieval sequence was deleted by homologous recombination. The mutant BiP mice died within several hours after birth due to impaired pulmonary surfactant biosynthesis and respiratory failure (29). We also found disordered layer formation in the cerebral cortex and cerebellum in the mutant BiP neonates. Although altered quality control in the ER due to mutant BiP may affect the expression of several proteins with regard to corticogenesis, we found that the expression of one such protein, reelin, secreted by Cajal-Retzius (CR) cells (9), was markedly reduced. These findings suggest that committed secretory cells, such as CR cells, have a threshold of

* Corresponding author. Mailing address: Department of Anesthesiology, Chiba University Graduate School of Medicine, 1-8-1 Inohana, Chuo-ku, Chiba City, Chiba 260-8670, Japan. Phone: 81-43-226-2573. Fax: 81-43-226-2156. E-mail: taoe@faculty.chiba-u.jp.
▽ Published ahead of print on 22 October 2007.

protein-folding capacity to cope with the normal physiological protein overload in the ER during development, and BiP plays an important role.

MATERIALS AND METHODS

Reagents. The following antibodies were used: mouse monoclonal antibody (mAb) CR50 against reelin (a gift from M. Ogawa, Brain Science Institute, RIKEN, Japan), rabbit antiserum against the hemagglutinin (HA) epitope (Zymed, San Francisco, CA), mouse mAb G10 against reelin, rabbit antiserum against Dab1 (Chemicon, Temecula, CA), rabbit antiserum against Dab1 (phospho-Y220) (Abcam, Cambridge, United Kingdom), mouse mAb EP5 against fibronectin, mouse mAb 6A6 against very-low-density lipoprotein receptor (VLDLR), rabbit antiserum against CHOP/GADD153, rabbit antiserum against ubiquitin, goat polyclonal antiserum against BiP/GRP78, mouse mAb J-3 against Cdk5 (Santa Cruz Biotechnology, Santa Cruz, CA), mouse mAb 9E10 against the Myc epitope (ATCC, Manassas, VA), mouse mAb against γ-tubulin (Sigma Chemical, St. Louis, MO), mouse mAb SPA-827 against BiP (KDEL sequence) (Stressgen, Ann Arbor, MI), Cy2-conjugated donkey antibody against rabbit immunoglobulin G (IgG), and Cy3-conjugated donkey antibody against mouse IgG (Jackson Immunoresearch Laboratories, West Grove, PA). TO-PRO-3 and a Slow-Fade antifade kit were purchased from Molecular Probes (Invitrogen, Carlsbad, CA).

Plasmids and transfection. A *reelin* cDNA (pCrl) was kindly provided by T. Curran (St. Jude Children's Research Hospital, Memphis, TN) (10). To express a Myc-tagged mutant BiP lacking the KDEL sequence, a cDNA encoding a mutant BiP with residues 1 to 650 was obtained by PCR using rat *BiP* cDNA (a gift from H. R. B. Pelham, MRC Laboratory of Molecular Biology, United Kingdom). The PCR product was subcloned into a pcDNA3.1 Myc-His vector (Invitrogen, Carlsbad, CA). Transfection was performed with the calcium phosphate method (20).

Mutant BiP mice. We used homologous recombination to establish knock-in mice expressing BiP lacking the carboxyl-terminal KDEL sequence (29). The missing KDEL sequence was replaced by an HA tag. All animal experimental procedures were performed in accordance with a protocol approved by the Institutional Animal Care Committee of Chiba University, Chiba, Japan.

Western blot. The brains removed from the mice and cells were homogenized in a buffer containing 0.4% Nonidet P-40, 0.2% *N*-lauroylsarcosine, 30 mM Tris-HCl (pH 8.0), 1 mM EDTA, 10 μg ml^{-1} aprotinin, 10 μg ml^{-1} leupeptin, and 30 μg ml^{-1} *N*-acetyl-L-leucinal-L-lecinal-L-norleucinal (ALLN; Sigma Chemical). The lysates were boiled in sodium dodecyl sulfate-polyacrylamide gel electrophoresis sample buffer and separated by sodium dodecyl sulfate-polyacrylamide gel electrophoresis under reducing conditions. Gels were transferred onto polyvinylidene fluoride membranes (Immobilon-P; Millipore Corp., Billerica, MA), blocked with 5% nonfat dry milk in the buffer described above, incubated with a primary antibody followed by peroxidase-conjugated donkey anti-goat, anti-mouse, or anti-rabbit IgG, and developed by chemiluminescence (ECL; Amersham Pharmacia Biotech, Buckinghamshire, United Kingdom). Imaging was obtained by using LAS1000 and Image Gauge software (Fuji Photo Film Co. Ltd., Tokyo, Japan).

Primary neuronal culture. Cortical neurons of mouse embryos were derived from embryos at day 17.5 to 18.5 according to standard procedures (1). After removing the meninges, cortical lobes were isolated in phosphate-buffered saline (PBS), dissected into small pieces, and digested with 0.25% trypsin and 0.02% DNase I in PBS with 5% glucose at 37°C for 20 min. Trypsin was then neutralized with a half volume of horse serum, and the solution was centrifuged at 440 × *g* for 5 min at 4°C. The resultant cells were triturated in Dulbecco's modified Eagle's medium (DMEM)–F-12 medium containing 10% fetal bovine serum using a siliconized Pasteur pipette and scattered at about 2×10^5 to 4×10^5 cells/cm^2 on plates coated with poly-L-lysine (Sigma). Cells were maintained in DMEM–F-12 medium containing 10% fetal bovine serum–1% penicillin-streptomycin for 3 days at 37°C and then replaced with opti-MEM (Invitrogen) containing 1% of an insulin-transferrin-selenium A mixture (ITS; Invitrogen) and antibiotics. On the following day, the supernatants were collected, centrifuged using a table-top machine at 440 × *g* for 5 min at 4°C, and concentrated by centrifugation (YM50; Millipore). The neurons were treated with control or reelin-containing medium (prepared as previously described) (8) at 37°C for 20 min and collected for Western blotting. 293T cells were transfected with full-length mouse reelin expression construct pCrl. The following day, the cells were washed with serum-free DMEM and maintained in opti-MEM containing 1% ITS and antibiotics. After three more days, the conditioned medium was collected, centrifuged at 440 × *g* for 5 min at 4°C, and used as the reelin-containing medium.

Confocal and immunofluorescence microscopy of primary neurons. Cells on coverslips were fixed in cold methanol for 10 min at −20°C and then processed as previously described (20). The stained cells were examined by either confocal laser scanning microscopy (LSM510 fitted with krypton and argon lasers; Carl Zeiss, Oberkochen, Germany) or fluorescence microscopy (Axiovert 200 M; Carl Zeiss).

Northern blot. Northern blot analysis was done as previously described (15). The expression level of the *reelin* and *BiP* mRNAs was assessed relative to that of β-*actin* mRNA using densitometry by Image Gauge software (Fuji Photo Film).

In situ hybridization histochemistry. *reelin* cDNA extending from nucleotides 4716 to 5476 (GenBank accession number U24703) (9) was cloned into the pGEM-T Easy vector (Promega, Madison, WI). In vitro transcription from *reelin* cDNA was performed using a digoxigenin-UTP RNA labeling kit (Roche Applied Science, Mannheim, Germany) to prepare the antisense and sense cRNA probes according to the manufacturer's instructions.

The brains of mouse embryos at embryonic day 15.5 (E15.5) were fixed with 4% paraformaldehyde dissolved in 0.1 M sodium phosphate buffer (pH 7.4), and postfixed overnight at 4°C with the same fixative. The brains were embedded in 2% agar in PBS and sliced coronally into 150-μm sections with a Microslicer (DTK-3000; Dosaka EM, Kyoto, Japan). Hybridization and detection procedures were performed as described below. The free-floating sections were incubated with proteinase K (20 μg/ml) in 0.1% Tween 20 in PBS (PBST) for 10 min at room temperature. Sections were rinsed with PBST, refixed in 4% paraformaldehyde for 20 min, and again rinsed with PBST three times each for 20 min. Sections were prehybridized in hybridization buffer (50% formamide, 5× SSC [1× SSC is 0.15 M NaCl plus 0.015 M sodium citrate], 50 μg/ml heparin, 0.1% Tween 20, 5 mg/ml torula RNA) for 30 min at 65°C. Subsequently, sections were hybridized overnight at 65°C with digoxigenin-UTP-labeled antisense or sense riboprobes (0.2 μg/ml) in the hybridization buffer. Sections were then sequentially rinsed in 2× SSCT (0.1% Tween 20 in SSC)–50% formamide twice each for 30 min at 65°C, 2× SSCT for 15 min at 65°C, and 0.2× SSCT twice each for 30 min at 65°C and then incubated overnight with alkaline phosphatase-coupled anti-digoxigenin antibody (1:4,000 dilution; Roche Applied Science, Mannheim, Germany). After washing with PBST three times and then once with 0.1 M Tris-HCl (pH 8.2), sections were stained by use of a solution prepared from FastRed tablets (Roche Applied Science, Mannheim, Germany) according to the manufacturer's instruction and then washed with PBST three times. Sections were then coverslipped with 80% glycerol, and fluorescence images were obtained directly with a confocal laser scanning microscope (LSM5 Pa; Zeiss, Oberkochen, Germany). No labeling was detectable in the control sections that were hybridized with the sense riboprobe (data not shown).

Immunohistochemistry. Pregnant mice were deeply anesthetized by Nembutal, and embryos were removed by cesarean section. The embryos were fixed by transcardiac perfusion with 4% paraformaldehyde in PBS, and the heads were further immersion fixed for 12 h at 4°C. Embryonic brains were then embedded in 3% agar in PBS, and sections at a thickness of 200 μm were prepared on a Microslicer (Dosaka EM, Kyoto, Japan). The sections were incubated with 10% normal goat serum in PBS for 30 min to block nonspecific antibody binding and then incubated with a mixture of CR50 mouse monoclonal antibody (1:200 dilution) (32) and rabbit anti-calretinin (1:2,000; Swant, Switzerland) in PBS for 12 h at 4°C. The sections were rinsed with PBS and then incubated with a mixture of Cy2-conjugated anti-rabbit IgG (1:100; Jackson Immunoresearch) and Cy3-conjugated anti-mouse IgG (1:200; Chemicon) in PBS for 2 h at 4°C. For calbindin immunohistochemistry of the cerebellum, rabbit anti-calbindin (1:2,000; Swant) was used as the primary antibody, and Cy2-conjugated anti-rabbit IgG was the secondary antibody. The sections were then rinsed with PBS and mounted onto glass slides with 80% glycerol. For counterstaining with a DNA dye, the sections immunostained with anti-calbindin antibody were stained with TO-PRO-3 (Invitrogen) and mounted with SlowFade (Molecular Probes). The sections were observed under a confocal laser scanning microscope (LSM5 Pa; Carl Zeiss).

BrdU labeling. Bromodeoxyuridine (BrdU) (80 mg · kg^{-1}) was administered intraperitoneally to pregnant mice at the E13 or E15 three times a day (at 10:00, 16:00, and 22:00). At E18, the embryos were removed by cesarean section and perfusion fixed as mentioned above. The brains were embedded in agar, and sections with a thickness of 200 μm were prepared and incubated with 2 N HCl for 1 h at room temperature. The sections were then rinsed with PBS, treated with 10% normal goat serum, and then incubated with a mouse mAb against BrdU (1:50; Becton Dickinson, San Jose, CA) for 12 h. After rinsing with PBS, the sections were incubated with Alexa 488-conjugated goat anti-mouse IgG

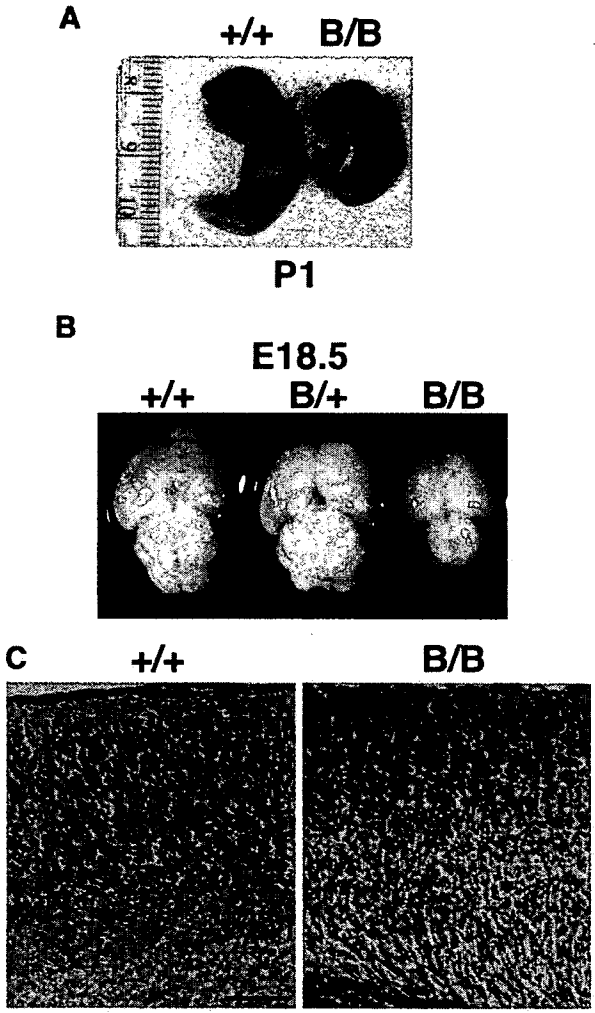

FIG. 1. Absence of the KDEL retrieval sequence from BiP impairs brain development. (A) Newborns at P1. (B) Brains from E18.5 embryos. (C) At E18, large numbers of neurons are distributed in the superficial layer of the mutant (right), in contrast to the cell-sparse layer I of the control (left). (C) Hematoxylin-eosin staining. Scale bar, 100 μm. B/B, homozygous; B/+, heterozygous; +/+, wild type.

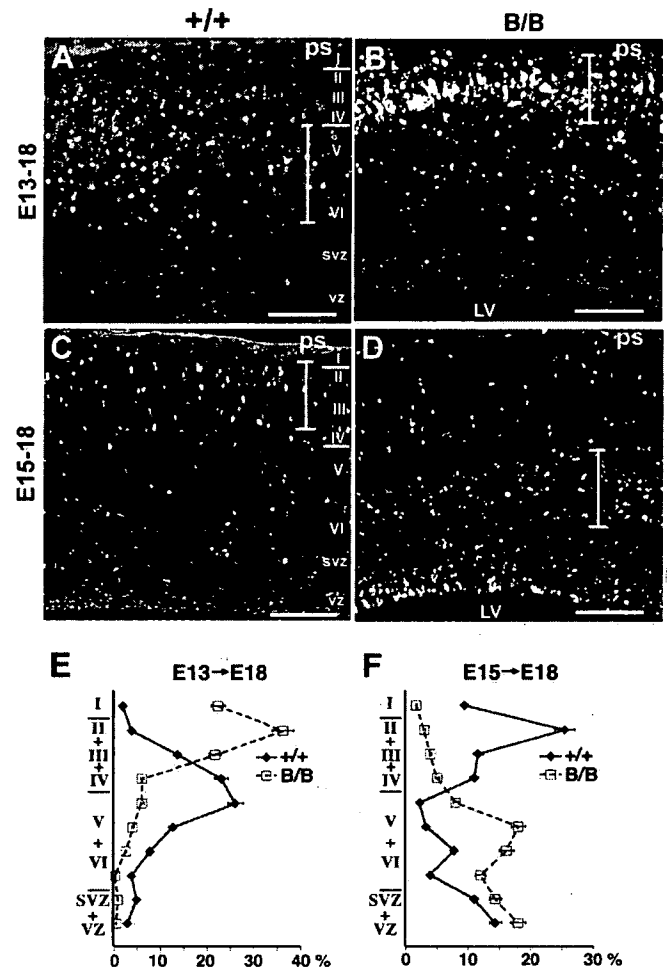

FIG. 2. Mutant BiP mice exhibit an outside-in pattern of neocortical layer formation. Shown is birth date analysis of the neocortical neurons. (A, B, and E) BrdU was administered at E13, and the distribution of the labeled cells was examined at E18. In control mice, heavily labeled cells were stratified in the lower layers (layers V and VI) (A), in contrast to the significant reduction of labeled cells in the lower layers and their significant increase in the superficial layer in the mutant (B). A quantitative analysis is represented in E. (C, D, and F) BrdU was administered at E15, and the distribution of the labeled cells was examined at E18. In the control, heavily labeled cells reached the upper layers (layers II and III), and the still-migrating cells were also found in the lower layer (C). In contrast, only small numbers of the labeled cells reached the upper layers (layers II and III), and a large proportion of them were distributed in the lower layer in the mutant (D). A quantitative analysis is represented in F. The graphs in E and F represent the averages ± standard errors of the means of BrdU-labeled cells in each layer of four serial sections from a representative brain of each genotype. The extent of the layers in that the cortical neurons were intensely labeled with BrdU is indicated by a vertical bar in each picture. B/B, homozygous mutant; +/+, wild-type mice; LV, lateral ventricle; ps, pial surface; svz, subventricular zone; vz, ventricular zone; I to VI, neocortical layers. Scale bars, 100 μm.

(1:500 dilution; Invitrogen) in PBS for 2 h at 4°C. The sections were then rinsed again with PBS and mounted onto glass slides with glycerol. Immunolocalization was observed under a confocal laser scanning microscope. The primordium of the somatosensory cortex was divided into 10 layers from the ventricular surface to the pial surface. The densities of BrdU-labeled cells in each layer were determined in four serial sections from a representative brain of each genotype. BrdU-labeled cells in the defined area of each section of the neocortical primordium were counted from the ventricular surface to the pial surface to obtain the total numbers of labeled cells, and the average percentages of the labeled cells in each layer were plotted on a histogram.

RESULTS

Defective neocortical layer formation in mutant BiP mice. The homozygous mutant BiP mice were born at the expected Mendelian ratio, and they died within 1 day after birth due to respiratory failure (29). They moved and responded to painful stimuli but appeared pale and were significantly smaller than wild-type mice (Fig. 1A). Among the various organs, the mutant brain, including the cerebral cortex and cerebellum, was substantially smaller than those of wild-type mice (Fig. 1B), suggesting that the brain was particularly affected by the BiP mutation. In fact, the neocortical stratification at E18, as observed with hematoxylin-eosin staining, was defective in the mutant BiP mice. The mutant brain had a relatively high density of neurons in neocortical layer I (Fig. 1C, right), in contrast

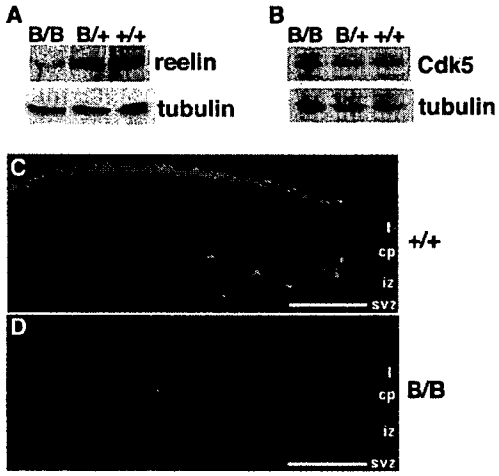

FIG. 3. Significant downregulation of reelin expression in superficial layer I of the mutant BiP neocortical primordium. (A and B) The levels of expression of reelin, Cdk5, and γ-tubulin in brains of E18.5 embryos were evaluated by Western blotting. (C and D) At E16, intense reelin immunoreactivity was found in the superficial layer of the control (C), but immunoreactivity was significantly reduced in the mutant brain (D). Scale bars, 200 μm. cp, cortical plate; iz, intermediate zone; svz, subventricular zone; I, layer I; B/B, homozygous mice; B/+, heterozygous mutant mice; +/+, wild-type mice.

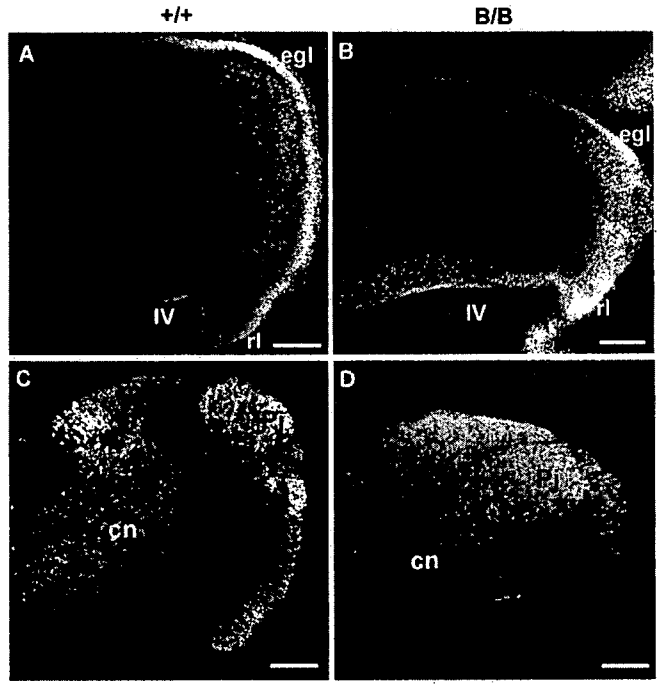

FIG. 4. Mutant BiP mice exhibit defective cerebellar development. (A and B) Staining of the cerebellar primordium at E18 with a DNA dye, TO-PRO-3. The cerebellum of the homozygote (B) is much smaller than that of the wild type (A). An EGL is formed in both genotypes, but the progression of EGL formation in the caudorostral direction is retarded in the homozygote (B). (C and D) Purkinje cell distribution in the cerebellum at E18. Calbindin-immunoreactive Purkinje cells are distributed in the cortical layer in the cerebellum of the control (C). In contrast, large numbers of immunoreactive cells stay in the subcortical region of the mutant cerebellum (D). Scale bars, 100 μm. B/B, homozygous mice; +/+, wild-type mice; cn, cerebellar nucleus; egl, EGL; Pj, Purkinje cell layer; rl, rhombic lip; IV, the fourth ventricle.

to a low density of neuronal arrangement in the control (Fig. 1C, left).

Cortical neurogenesis occurs in the ventricular zone, and the new neurons migrate through other new neurons to the marginal zone and then move to their final destination during embryogenesis. To further investigate the defect in layer formation during neocortical development, birth date analysis of the neocortical neurons was carried out by BrdU labeling (Fig. 2A to D). Neuronal precursors in the ventricular zone became labeled with BrdU during proliferation and migrated after the final mitosis through earlier-born neurons to the cortical plate in normal corticogenesis. When BrdU was administered at E13, heavily labeled cells were distributed in forming layers V and VI, and lightly labeled cells that repeated mitosis after BrdU incorporation were distributed in the upper layers at E18 in the control (Fig. 2A and E), as reported previously by Caviness (7). In the mutant, however, heavily labeled cells were distributed in the upper layer up to superficial layer I, and few labeled cells were observed in the lower layer at E18 (Fig. 2B and E). When BrdU was administered at E15, in the control, the heavily labeled cells reached upper layers II and III at E18 (Fig. 2C and F), as reported previously by Caviness (7), but in the mutant, only a small number of heavily labeled cells reached these upper layers, and most of the labeled cells were distributed in the lower layer (Fig. 2D and F). These findings indicate that, in the mutant brain, the earlier-born neurons reached the superficial layer and remained there and that the later-born neurons did not reach the upper layer, remaining in the lower layer. The mutant BiP mice exhibited an outside-in pattern of neocortical layer formation, in contrast to the inside-out pattern in the control (7), indicating that neocortical layer formation was impaired.

Mutant BiP mice have reduced expression of reelin. The above-described findings suggested that aberrant neocortical formation is due to the defects in layer formation, like a deficiency in reelin signaling in a *reeler* mutant malformation (9, 13) or a deficiency in Cdk5 signaling (33). Indeed, analysis of the embryonic cerebral neocortex revealed significantly reduced reelin expression by Western blotting and immunoreactivity in superficial layer I of the mutant BiP mice (Fig. 3A, C, and D), while the expression of Cdk5 was preserved (Fig. 3B). These results are consistent with the fact that reelin is a secretory protein that may interact with BiP in the ER, whereas Cdk5 is a cytosolic protein that is apart from BiP.

Because *reeler* malformation is also well documented in the cerebellum with regard to the migration defect of Purkinje cells (48), the structure of the cerebellum was examined at E18. The growth of the mutant cerebellum was significantly retarded as shown by staining with DNA dye (Fig. 4A and B). Although the external granular layer (EGL) was formed in both genotypes, the development of an EGL migrating tangentially from the rhombic lip was significantly retarded in the mutant BiP mice (Fig. 4A and B). A large number of Purkinje cells remained in the subcortical region, in contrast to the cortical arrangement of Purkinje cells in the control (Fig. 4C and D). Hippocampal layer formation showed little defect in the mutant BiP mice based on hematoxylin-eosin-stained sections (data not shown).

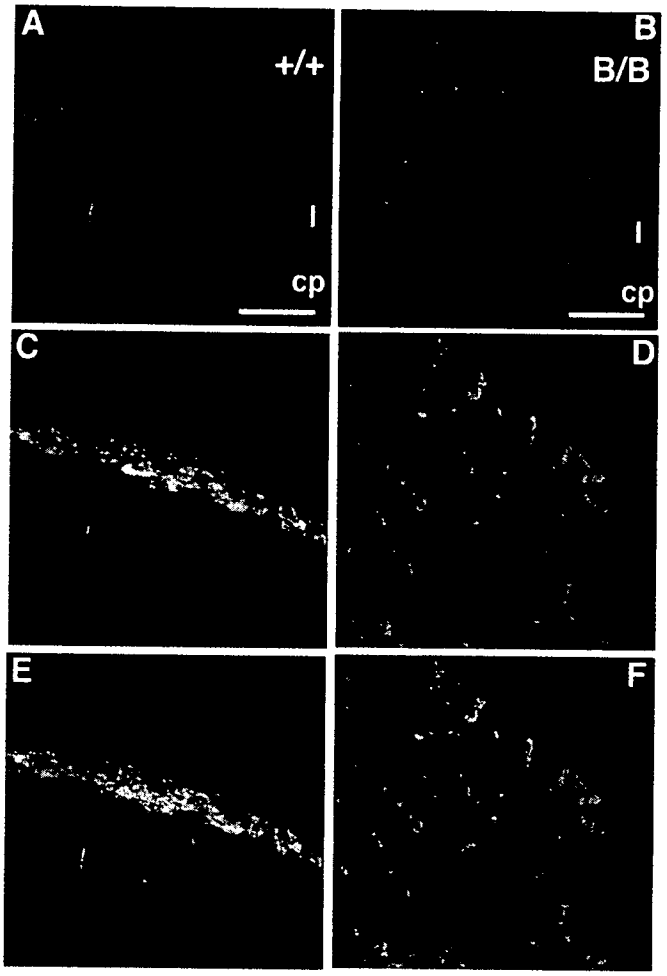

FIG. 5. Distribution of CR cells in the neocortical primordium. At E16, reelin immunoreactivity (red) in the superficial layer (I) of control (A) and mutant (B) brains was present. Calretinin-immunopositive CR cells (green) were found in the superficial layers of both control (C) and mutant (D) mice. Reelin immunoreactivity colocalizes with calretinin in CR cells in the control (E) (A and C were merged), but reelin immunoreactivity is hardly detectable in the calretinin-positive cells in superficial layer I of the mutant (F) (B and D were merged). Furthermore, the cells that were double labeled with reelin and calretinin were found in the layers below the superficial layer in the mutant (F), although such cells were not detected in the wild type (E). Scale bars, 50 μm.

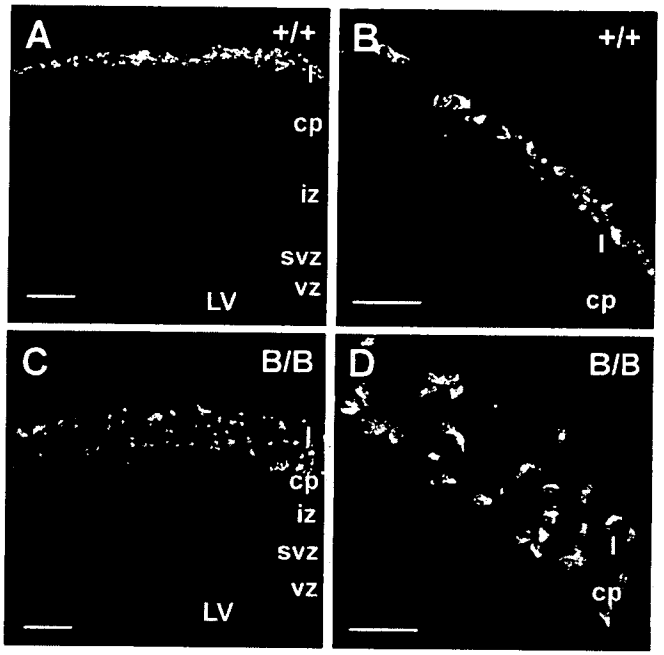

FIG. 6. The cells positive for *reelin* mRNA were scattered in the neocortical primordium of mutant BiP mice. The distribution of CR cells was further confirmed by in situ hybridization for *reelin* mRNA as the marker of CR cells in the neocortical primordium at E15.5. In the control, *reelin* mRNA-positive cells were situated in the superficial layer (layer I) as shown in A. The higher magnification of the upper cortical area represents the characteristic horizontal arrangement of CR cells (B). In contrast, *reelin* mRNA-positive cells were distributed from the superficial layer into the cortical plate in the homozygote (C). (D) Higher magnification of the upper cortical area in C. The random orientation of *reelin*-positive cells is evident. Scale bars, 100 μm in A and C and 50 μm in B and D.

The structure of the superficial layer of the neocortical primordium was further examined by double immunohistochemical labeling for both reelin and calretinin. Calretinin-immunopositive neurons, corresponding to CR cells in the neocortical primordium, were found in the superficial layer of the mutant BiP mice, but their numbers were significantly reduced, and reelin immunoreactivity was barely detected (Fig. 5B, D, and F), in contrast to the localization of reelin immunoreactivity in the calretinin-positive neurons in superficial layer I of the wild-type mice (Fig. 5A, C, and E). Some of calretinin-immunopositive CR cells of the mutant neocortex appeared in a disorganized, scattered pattern other than the marginal zone (Fig. 5F). This finding was confirmed by in situ hybridization histochemistry of the neocortical primordium by using *reelin* cRNA probe as the marker for CR cells. The cells positive for *reelin* mRNA formed a thin superficial layer in wild-type mice (Fig. 6A and B). In contrast, the cells positive for *reelin* mRNA were scattered in the upper layer of the neocortical primordium of the mutant BiP mice (Fig. 6C and D). These findings of in situ hybridization histochemistry correspond well with those of calretinin-immunoreactive cells. Furthermore, the present findings indicate that the transcription of the *reelin* gene takes place to a similar degree in both mutant and wild-type mice, but the reelin protein is significantly reduced in the CR cells of the mutant.

While this mouse does have features of a *reeler* mutant phenotype, such as an outside-in pattern of neocortical layer formation and the migration defect of Purkinje cells in the cerebellum, it also has other phenotypes in the brain that are distinct from the *reeler* phenotype. These include the reduction in the size of the whole brain and the apparent scattering of reelin- and calretinin-positive neurons throughout the cortex. This is not surprising since BiP likely has a multitude of substrates that are significant for brain development. Among them, we decided to focus on reelin since at least one of the reeler mutants has a defect in intracellular transport of reelin (11) rather than the production of reelin, and the transport mutant BiP may affect the folding and secretion of reelin.

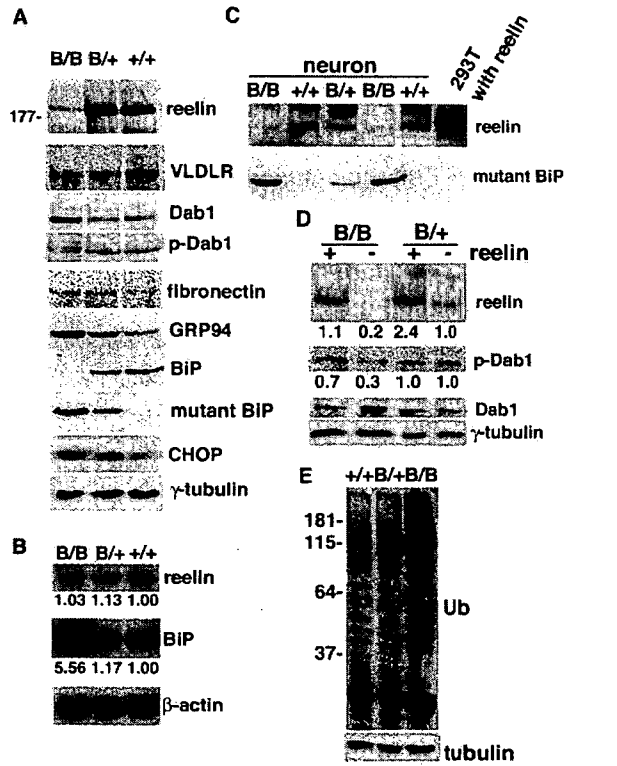

FIG. 7. Reelin expression is reduced posttranscriptionally in the mutant BiP brain. (A) The levels of expression of reelin, VLDLR, Dab1, tyrosine-phosphorylated Dab1 (p-Dab1), fibronectin, GRP94, BiP, mutant BiP, CHOP, and γ-tubulin in brains of E18.5 embryos were evaluated by Western blotting. In mutant BiP, the carboxyl-terminal KDEL sequence was replaced by an HA tag. (B) Northern blotting using probes for reelin, BiP, and β-actin mRNAs in brains at E18.5. The expression levels of reelin and BiP mRNAs were assessed by the relative ratio to β-actin mRNA. (C) Secretion of reelin and mutant BiP in the culture medium from the primary neurons and 293T cells transfected with reelin cDNA, as evaluated by Western blotting. (D) Primary neurons were treated with control (−) or reelin-containing medium (+) at 37°C for 20 min, collected, and subjected to Western blotting with antibodies against reelin, Dab1, tyrosine-phosphorylated Dab1, and γ-tubulin. The expression levels of reelin and tyrosine-phosphorylated Dab1 were assessed by the relative ratios to γ-tubulin. (E) Expression of ubiquitinated (Ub) proteins in the cerebrum at E18.5 embryos, as evaluated by Western blotting. B/B, homozygous mice; B/+, heterozygous mutant mice; +/+, wild-type mice.

Reelin secretion is impaired in the mutant BiP brain. Reelin is a large secreted glycoprotein (9) produced by some cortical neurons such as CR cells in the marginal zone during development. Reelin mediates cortical laminar formation through binding to VLDLR and apolipoprotein E receptor type 2 (ApoER2) on cortical neurons (8, 43). In *reeler* mice deficient in the reelin gene (9), the cortical neurons lack the ability to localize properly and settle inside the earlier-migrating neurons (7).

In E18.5 mice, we used an antibody directed against the amino terminus of reelin to detect a fragment of reelin (~180 kDa) in the wild-type cerebral cortex; however, these fragments were much less intense in the homozygous mutant BiP cortex (Fig. 7A), consistent with histological observations. Although VLDLR expression was equivalent between wild-type and mutant BiP cortices, dephosphorylated Dab1 accumulated in the mutant BiP brain, indicating that the reelin signaling pathway was inactivated there. The expression of another secreted glycoprotein, fibronectin, was preserved in the mutant brain. The reelin deficiency was not a consequence of reduced transcription, because *reelin* mRNA expression did not differ in control and mutant brains (Fig. 7B), consistent with the in situ hybridization experiment (Fig. 6). The expression of *BiP* mRNA as well as CHOP protein (a cell death-related transcriptional factor of the UPR) (50) was enhanced in the mutant brain (Fig. 7A and B), suggesting that the mutant brain suffered from ER stress.

Mutant BiP might impair the folding of reelin, leading to its degradation by the ER-associated degradation pathway or to its secretion as an immature form from the CR cells due to an escape from ER quality control. To test this possibility, we used primary neurons derived from embryonic brains and found a significant decrease in reelin secretion by the homozygous mutant BiP neurons compared with that of wild-type or heterozygous neurons (Fig. 7C). To investigate whether the homozygous mutant BiP neurons maintained their responsiveness to reelin stimulation, we incubated primary neurons with conditioned culture medium containing a severalfold physiological level of reelin secreted by 293T cells transiently transfected with reelin cDNA (Fig. 7D). Exogenous reelin seemed to be active on the homozygous neurons, leading to the activation of the reelin signaling pathway, as demonstrated by a reduced amount of Dab1 expression and an increased amount of phospho-Dab1 expression. On the other hand, the reelin signaling pathway in the heterozygous mutant cortical neurons seems to be constitutively active with endogenous reelin even without exogenous reelin stimulation. Thus, Dab1 expression and phosphorylation (Fig. 7D) are rather unchanged in the heterozygous mutant. These results suggest that the impaired secretion of reelin by the CR cells rather than defective responsiveness in the cortical neurons may be responsible for the neurological phenotype of *reeler* mutant-like malformations in mutant BiP mice. Thus, the impaired retrieval of BiP may promote the degradation of misfolded proteins by the ubiquitin/proteasome pathway. In fact, ubiquitinated proteins accumulated in the mutant cerebrum (Fig. 7E).

BiP may enhance the folding of reelin. Mutant BiP was detected in the ER (29), but a significant fraction was also secreted from cells because of the lack of the retrieval motif (KDEL) (Fig. 7C). We examined the subcellular localization of reelin to establish its relationship with mutant and wild-type BiP. Reelin colocalized with mutant BiP in the ER in primary neurons derived from heterozygous mutant BiP embryos; this was also the case in cortical neurons in the homozygous mutant postnatal brain, where the expression of reelin was reduced (Fig. 8A). To obtain further insight into the interaction of BiP and reelin, we performed cotransfection experiments in HeLa cells. Coexpression of reelin and wild-type BiP, but not the mutant BiP lacking the KDEL sequence, greatly enhanced the expression of reelin protein (reelin mRNA levels were equivalent in the two transfections) (Fig. 8B). These results suggest that BiP promotes the folding of reelin.

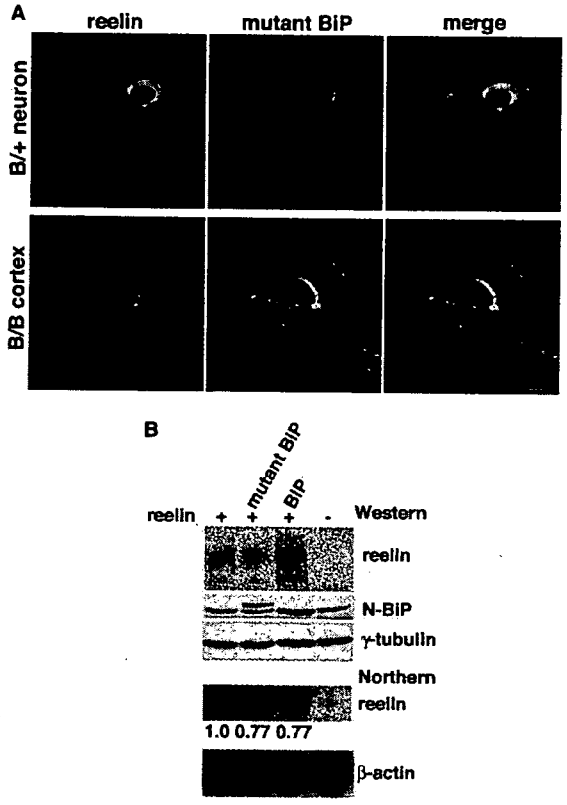

FIG. 8. BiP may enhance the maturation of reelin. (A) Subcellular localization of endogenous reelin and mutant BiP in primary neurons from the heterozygous (B/+) mutant BiP embryo and the cortex of the homozygous (B/B) mutant BiP embryo (E18.5), as evaluated by confocal laser scanning microscopy, with double labeling using a mouse mAb for reelin and a rabbit antiserum for HA. Scale bars, 10 μm. (B) HeLa cells were transiently transfected with reelin alone or co-transfected with either mutant BiP in which the KDEL sequence was replaced by a Myc tag or wild-type BiP (the Myc-tagged mutant BiP has a higher molecular weight than wild-type BiP). The levels of expression of reelin, BiP, and γ-tubulin were evaluated by Western blotting, and the levels of expression of *reelin* and β-*actin* mRNA were evaluated by Northern blotting. The expression level of *reelin* mRNA was assessed relative to that of β-*actin* mRNA.

DISCUSSION

We produced knock-in mice expressing a mutant BiP with the retrieval sequence deleted, which allowed us to examine the effects of a defect in the response to secretory pathway stress without completely eliminating BiP function, as would be the case with BiP knockout mice (28). The loss of BiP function was compensated for by the UPR in embryonic fibroblasts. However, neonates expressing mutant BiP suffered respiratory failure caused by the impaired secretion of pulmonary surfactant in alveolar type II epithelial cells (29). Furthermore, we observed abnormal corticogenesis in mutant BiP mice. Mutant BiP may predominantly affect dedicated secretory cells, such as alveolar type II cells and CR cells, in which active secretion is particularly important; thus, protein folding was probably affected in these cells. Indeed, we found an impaired secretion of reelin in CR cells, which may account for one aspect of cortical malformation in the cerebrum and cerebellum of mutant BiP mice. We also demonstrated increased Dab1 protein levels and a reduction in Dab1 tyrosine phosphorylation, which are consistent with a *reeler*-like phenotype. On the other hand, this mouse has other phenotypes in the brain that are distinct from the *reeler* phenotype. These include the reduction in the size of the whole brain and the apparent scattering of CR cells throughout the cortex, suggesting that mutant BiP may likely interfere with other substrates in addition to the reelin required for brain development.

The deletion of the retrieval sequence from BiP could have two possible effects. First, the lack of recycling of mutant BiP to the ER could impair the folding environment in the ER. This effect may be limited because constitutively active UPR compensates for it, and a sufficient amount of the functional mutant BiP, as long as it stays in the ER, may be produced for cell survival. Second, the impaired retrieval of mutant BiP may affect quality control in post-ER compartments. In addition to the ER itself, several studies have revealed that proper ER-to-Golgi apparatus transport and the subsequent retrieval/return of proteins and lipids to the ER may contribute to quality control (16, 19, 42, 45, 47). In this regard, the folding (and therefore function) of reelin may be dependent on the proper retrieval of BiP to the ER via interactions with the KDEL receptor.

Reelin is a large 3,461-residue secreted glycoprotein that has eight reelin repeats of ~350 residues each that contain an epidermal growth factor motif followed by a carboxyl-terminal 33 residues rich in basic amino acids (43). During embryogenesis, CR cells secrete reelin as homo-oligomers that function in cortical layer formation through binding to lipoprotein receptors on cortical neurons (44). Although the folding, intracellular transport, and oligomerization of reelin have not been characterized in detail, we found that reelin protein expression was impaired in mutant BiP mice, indicating that BiP may play a role in the maturation of reelin. Furthermore, we found that the expression levels of BiP mRNA and the CHOP protein were enhanced in the mutant brain, suggesting that the mutant brain might have suffered from ER stress. We speculate that the folding of the reelin protein may be vulnerable to impaired quality control in the ER and the post-ER compartments of mutant CR cells. If true, this assumption suggests that environmental stresses that perturb ER quality control may also impair the reelin signaling pathway and other factors, which may cause neuronal migration defects.

In addition to brain development, several studies suggested the possible role of reelin in the pathogenesis of human mental disorders such as schizophrenia, autism, bipolar disorder, and Alzheimer's disease (5, 14, 43). Because reelin signaling through ApoER2 in adult brains modulates synaptic plasticity and memory formation (2), the defective reelin signaling pathway may contribute to the pathogenesis of adult mental disorders. Reelin and ApoE share ApoER2 on cortical neurons (8), and ApoE inhibits reelin signaling by competing for binding to ApoER2. Interestingly, the E4 allele of ApoE increases the risk of developing sporadic forms of Alzheimer's disease.

In the meantime, the persistent accumulation of misfolded proteins beyond the capacity of ER quality control causes ER stress, leading to cellular dysfunction and cell death (24, 26). This process is thought to cause human mental disorders such as neurodegenerative diseases including Alzheimer's disease (23) and Parkinson's disease (21), bipolar disorders (22), and

ischemic neuronal injury (41). The involvement of impaired BiP function in neurodegenerative diseases has been reported in a mouse model where the disruption of SIL1, a cochaperone of BiP, caused protein accumulation and neurodegeneration (49). Thus, reelin signaling and ER quality control may be related to the pathogenesis of adult mental disorders, as seen in reeler mutant-like cerebral malformation in mutant BiP neonates.

The UPR is a ubiquitous mechanism in all cells to adapt to ER stress in pathological conditions, and BiP is an essential component of this system. Our results suggest that a physiological increase in the production of reelin and other factors in dedicated secretory cells like CR cells during neonatal periods may require the UPR and a proper folding capacity in the ER. Neuronal migration and stratification may be sensitive to environmental insults such as viral infection, hypoxia, and ischemia that perturb ER functions.

ACKNOWLEDGMENTS

We thank T. Nishino, K. Toshimori, and T. Yamashita for critical comments. We also thank M. Kashio for excellent technical assistance.

This work was supported by grants-in-aid for science research from the Ministry of Education, Culture, Sports, Science, and Technology of Japan to T.A. and grant 05-32 from NIBIO to S.Y.

REFERENCES

1. **Banker, G., and K. Goslin.** 1988. Developments in neuronal cell culture. Nature **336**:185–186.
2. **Beffert, U., E. J. Weeber, A. Durudas, S. Qiu, I. Masiulis, J. D. Sweatt, W. P. Li, G. Adelmann, M. Frotscher, R. E. Hammer, and J. Herz.** 2005. Modulation of synaptic plasticity and memory by Reelin involves differential splicing of the lipoprotein receptor Apoer2. Neuron **47**:567–579.
3. **Beh, C. T., and M. D. Rose.** 1995. Two redundant systems maintain levels of resident proteins within the yeast endoplasmic reticulum. Proc. Natl. Acad. Sci. USA **92**:9820–9823.
4. **Bonifacino, J. S., and A. M. Weissman.** 1998. Ubiquitin and the control of protein fate in the secretory and endocytic pathways. Annu. Rev. Cell Dev. Biol. **14**:19–57.
5. **Bothwell, M., and E. Giniger.** 2000. Alzheimer's disease: neurodevelopment converges with neurodegeneration. Cell **102**:271–273.
6. **Brodsky, J. L., and A. A. McCracken.** 1999. ER protein quality control and proteasome-mediated protein degradation. Semin. Cell Dev. Biol. **10**:507–513.
7. **Caviness, V. S., Jr.** 1982. Neocortical histogenesis in normal and reeler mice: a developmental study based upon [3H]thymidine autoradiography. Brain Res. **256**:293–302.
8. **D'Arcangelo, G., R. Homayouni, L. Keshvara, D. S. Rice, M. Sheldon, and T. Curran.** 1999. Reelin is a ligand for lipoprotein receptors. Neuron **24**:471–479.
9. **D'Arcangelo, G., G. G. Miao, S. C. Chen, H. D. Soares, J. I. Morgan, and T. Curran.** 1995. A protein related to extracellular matrix proteins deleted in the mouse mutant *reeler*. Nature **374**:719–723.
10. **D'Arcangelo, G., K. Nakajima, T. Miyata, M. Ogawa, K. Mikoshiba, and T. Curran.** 1997. Reelin is a secreted glycoprotein recognized by the CR-50 monoclonal antibody. J. Neurosci. **17**:23–31.
11. **de Bergeyck, V., K. Nakajima, C. Lambert de Rouvroit, B. Naerhuyzen, A. M. Goffinet, T. Miyata, M. Ogawa, and K. Mikoshiba.** 1997. A truncated Reelin protein is produced but not secreted in the 'Orleans' reeler mutation (Reln[rl-Orl]). Brain Res. Mol. Brain Res. **50**:85–90.
12. **Ellgaard, L., and A. Helenius.** 2003. Quality control in the endoplasmic reticulum. Nat. Rev. Mol. Cell Biol. **4**:181–191.
13. **Falconer, D. S.** 1951. Two new mutant, 'trembler' and 'reeler,' with neurological actions in the house mouse (Mus muscululus L.). J. Genet. **50**:192–201.
14. **Fatemi, S. H.** 2005. Reelin glycoprotein: structure, biology and roles in health and disease. Mol. Psych. **10**:251–257.
15. **Hamada, H., M. Suzuki, S. Yuasa, N. Mimura, N. Shinozuka, Y. Takada, T. Nishino, H. Nakaya, H. Koseki, and T. Aoe.** 2004. Dilated cardiomyopathy caused by aberrant endoplasmic reticulum quality control in mutant KDEL receptor transgenic mice. Mol. Cell. Biol. **24**:8007–8017.
16. **Hammond, C., and A. Helenius.** 1994. Quality control in the secretory pathway: retention of a misfolded viral membrane glycoprotein involves cycling between the ER, intermediate compartment, and Golgi apparatus. J. Cell Biol. **126**:41–52.
17. **Harding, H. P., and D. Ron.** 2002. Endoplasmic reticulum stress and the development of diabetes: a review. Diabetes **51**(Suppl. 3):S455–S461.
18. **Harding, H. P., Y. Zhang, and D. Ron.** 1999. Protein translation and folding are coupled by an endoplasmic-reticulum-resident kinase. Nature **397**:271–274.
19. **Haynes, C. M., S. Caldwell, and A. A. Cooper.** 2002. An HRD/DER-independent ER quality control mechanism involves Rsp5p-dependent ubiquitination and ER-Golgi transport. J. Cell Biol. **158**:91–101.
20. **Hsu, V. W., N. Shah, and R. D. Klausner.** 1992. A brefeldin A-like phenotype is induced by the overexpression of a human ERD-2-like protein, ELP-1. Cell **69**:625–635.
21. **Imai, Y., M. Soda, H. Inoue, N. Hattori, Y. Mizuno, and R. Takahashi.** 2001. An unfolded putative transmembrane polypeptide, which can lead to endoplasmic reticulum stress, is a substrate of Parkin. Cell **105**:891–902.
22. **Kakiuchi, C., K. Iwamoto, M. Ishiwata, M. Bundo, T. Kasahara, I. Kusumi, T. Tsujita, Y. Okazaki, S. Nanko, H. Kunugi, T. Sasaki, and T. Kato.** 2003. Impaired feedback regulation of XBP1 as a genetic risk factor for bipolar disorder. Nat. Genet. **35**:171–175.
23. **Katayama, T., K. Imaizumi, N. Sato, K. Miyoshi, T. Kudo, J. Hitomi, T. Morihara, T. Yoneda, F. Gomi, Y. Mori, Y. Nakano, J. Takeda, T. Tsuda, Y. Itoyama, O. Murayama, A. Takashima, P. St. George-Hyslop, M. Takeda, and M. Tohyama.** 1999. Presenilin-1 mutations downregulate the signalling pathway of the unfolded-protein response. Nat. Cell Biol. **1**:479–485.
24. **Kaufman, R. J.** 2002. Orchestrating the unfolded protein response in health and disease. J. Clin. Investig. **110**:1389–1398.
25. **Kleizen, B., and I. Braakman.** 2004. Protein folding and quality control in the endoplasmic reticulum. Curr. Opin. Cell Biol. **16**:343–349.
26. **Kopito, R. R., and D. Ron.** 2000. Conformational disease. Nat. Cell Biol. **2**:E207–E209.
27. **Lewis, M. J., and H. R. Pelham.** 1990. A human homologue of the yeast HDEL receptor. Nature **348**:162–163.
28. **Luo, S., C. Mao, B. Lee, and A. S. Lee.** 2006. GRP78/BiP is required for cell proliferation and protecting the inner cell mass from apoptosis during early mouse embryonic development. Mol. Cell. Biol. **26**:5688–5697.
29. **Mimura, N., H. Hamada, M. Kashio, H. Jin, Y. Toyama, K. Kimura, M. Iida, S. Goto, H. Saisho, K. Toshimori, H. Koseki, and T. Aoe.** 2007. Aberrant quality control in the endoplasmic reticulum impairs the biosynthesis of pulmonary surfactant in mice expressing mutant BiP. Cell Death Differ. **14**:1475–1485.
30. **Munro, S., and H. R. Pelham.** 1987. A C-terminal signal prevents secretion of luminal ER proteins. Cell **48**:899–907.
31. **Munro, S., and H. R. Pelham.** 1986. An Hsp70-like protein in the ER: identity with the 78 kd glucose-regulated protein and immunoglobulin heavy chain binding protein. Cell **46**:291–300.
32. **Ogawa, M., T. Miyata, K. Nakajima, K. Yagyu, M. Seike, K. Ikenaka, H. Yamamoto, and K. Mikoshiba.** 1995. The reeler gene-associated antigen on Cajal-Retzius neurons is a crucial molecule for laminar organization of cortical neurons. Neuron **14**:899–912.
33. **Ohshima, T., J. M. Ward, C. G. Huh, G. Longenecker, Veeranna, H. C. Pant, R. O. Brady, L. J. Martin, and A. B. Kulkarni.** 1996. Targeted disruption of the cyclin-dependent kinase 5 gene results in abnormal corticogenesis, neuronal pathology and perinatal death. Proc. Natl. Acad. Sci. USA **93**:11173–11178.
34. **Oyadomari, S., A. Koizumi, K. Takeda, T. Gotoh, S. Akira, E. Araki, and M. Mori.** 2002. Targeted disruption of the Chop gene delays endoplasmic reticulum stress-mediated diabetes. J. Clin. Investig. **109**:525–532.
35. **Patil, C., and P. Walter.** 2001. Intracellular signaling from the endoplasmic reticulum to the nucleus: the unfolded protein response in yeast and mammals. Curr. Opin. Cell Biol. **13**:349–355.
36. **Reimold, A. M., A. Etkin, I. Clauss, A. Perkins, D. S. Friend, J. Zhang, H. F. Horton, A. Scott, S. H. Orkin, M. C. Byrne, M. J. Grusby, and L. H. Glimcher.** 2000. An essential role in liver development for transcription factor XBP-1. Genes Dev. **14**:152–157.
37. **Reimold, A. M., N. N. Iwakoshi, J. Manis, P. Vallabhajosyula, E. Szomolanyi-Tsuda, E. M. Gravallese, D. Friend, M. J. Grusby, F. Alt, and L. H. Glimcher.** 2001. Plasma cell differentiation requires the transcription factor XBP-1. Nature **412**:300–307.
38. **Scheuner, D., B. Song, E. McEwen, C. Liu, R. Laybutt, P. Gillespie, T. Saunders, S. Bonner-Weir, and R. J. Kaufman.** 2001. Translational control is required for the unfolded protein response and in vivo glucose homeostasis. Mol. Cell **7**:1165–1176.
39. **Schroder, M., and R. J. Kaufman.** 2005. The mammalian unfolded protein response. Annu. Rev. Biochem. **74**:739–789.
40. **Sonnichsen, B., J. Fullekrug, P. N. Van, W. Diekmann, D. G. Robinson, and G. Mieskes.** 1994. Retention and retrieval: both mechanisms cooperate to maintain calreticulin in the endoplasmic reticulum. J. Cell Sci. **107**:2705–2717.
41. **Tajiri, S., S. Oyadomari, S. Yano, M. Morioka, T. Gotoh, J. I. Hamada, Y. Ushio, and M. Mori.** 2004. Ischemia-induced neuronal cell death is mediated by the endoplasmic reticulum stress pathway involving CHOP. Cell Death Differ. **11**:403–415.

42. **Taxis, C., F. Vogel, and D. H. Wolf.** 2002. ER-Golgi traffic is a prerequisite for efficient ER degradation. Mol. Biol. Cell **13**:1806–1818.
43. **Tissir, F., and A. M. Goffinet.** 2003. Reelin and brain development. Nat. Rev. Neurosci. **4**:496–505.
44. **Utsunomiya-Tate, N., K. Kubo, S. Tate, M. Kainosho, E. Katayama, K. Nakajima, and K. Mikoshiba.** 2000. Reelin molecules assemble together to form a large protein complex, which is inhibited by the function-blocking CR-50 antibody. Proc. Natl. Acad. Sci. USA **97**:9729–9734.
45. **Vashist, S., and D. T. Ng.** 2004. Misfolded proteins are sorted by a sequential checkpoint mechanism of ER quality control. J. Cell Biol. **165**:41–52.
46. **Wu, J., and R. J. Kaufman.** 2006. From acute ER stress to physiological roles of the unfolded protein response. Cell Death Differ. **13**:374–384.
47. **Yamamoto, K., R. Fujii, Y. Toyofuku, T. Saito, H. Koseki, V. W. Hsu, and T. Aoe.** 2001. The KDEL receptor mediates a retrieval mechanism that contributes to quality control at the endoplasmic reticulum. EMBO J. **20**:3082–3091.
48. **Yuasa, S., J. Kitoh, S. Oda, and K. Kawamura.** 1993. Obstructed migration of Purkinje cells in the developing cerebellum of the reeler mutant mouse. Anat. Embryol. (Berlin) **188**:317–329.
49. **Zhao, L., C. Longo-Guess, B. S. Harris, J. W. Lee, and S. L. Ackerman.** 2005. Protein accumulation and neurodegeneration in the woozy mutant mouse is caused by disruption of SIL1, a cochaperone of BiP. Nat. Genet. **37**:974–979.
50. **Zinszner, H., M. Kuroda, X. Wang, N. Batchvarova, R. T. Lightfoot, H. Remotti, J. L. Stevens, and D. Ron.** 1998. CHOP is implicated in programmed cell death in response to impaired function of the endoplasmic reticulum. Genes Dev. **12**:982–995.

nature medicine

Nucleotide-sugar transporter SLC35D1 is critical to chondroitin sulfate synthesis in cartilage and skeletal development in mouse and human

Shuichi Hiraoka[1,13], Tatsuya Furuichi[2,13], Gen Nishimura[3], Shunichi Shibata[4], Masaki Yanagishita[5], David L Rimoin[6], Andrea Superti-Furga[7], Peter G Nikkels[8], Minako Ogawa[1], Kayoko Katsuyama[1], Hidenao Toyoda[9–11], Akiko Kinoshita-Toyoda[9,10], Nobuhiro Ishida[12], Kyoichi Isono[1], Yutaka Sanai[12], Daniel H Cohn[6], Haruhiko Koseki[1] & Shiro Ikegawa[2]

Proteoglycans are a family of extracellular macromolecules comprised of glycosaminoglycan chains of a repeated disaccharide linked to a central core protein[1,2]. Proteoglycans have critical roles in chondrogenesis and skeletal development. The glycosaminoglycan chains found in cartilage proteoglycans are primarily composed of chondroitin sulfate[3]. The integrity of chondroitin sulfate chains is important to cartilage proteoglycan function; however, chondroitin sulfate metabolism in mammals remains poorly understood. The solute carrier-35 D1 (SLC35D1) gene (*SLC35D1*) encodes an endoplasmic reticulum nucleotide-sugar transporter (NST) that might transport substrates needed for chondroitin sulfate biosynthesis[4,5]. Here we created *Slc35d1*-deficient mice that develop a lethal form of skeletal dysplasia with severe shortening of limbs and facial structures. Epiphyseal cartilage in homozygous mutant mice showed a decreased proliferating zone with round chondrocytes, scarce matrices and reduced proteoglycan aggregates. These mice had short, sparse chondroitin sulfate chains caused by a defect in chondroitin sulfate biosynthesis. We also identified that loss-of-function mutations in human *SLC35D1* cause Schneckenbecken dysplasia, a severe skeletal dysplasia. Our findings highlight the crucial role of NSTs in proteoglycan function and cartilage metabolism, thus revealing a new paradigm for skeletal disease and glycobiology.

Chondroitin sulfate chains consist of repeating disaccharide units of *N*-acetylgalactosamine (GalNAc) and glucuronic acid (GlcUA), which are sulfated at either the C6 or C4 position of GalNAc[3]. The integrity of the chondroitin sulfate chain is maintained by elongation (biosynthesis) of the chain and by sulfation of GalNAc. It has been suggested that the chondroitin sulfate status of proteoglycan modulates its functions in epiphyseal cartilage. In humans, after skeletal maturation and concurrent with the disappearance of epiphyseal cartilage, chondroitin sulfate chain length decreases by more than half, and the ratio of C6 to C4 sulfation in chondroitin sulfate increases more than 20-fold[6]. These findings suggest that the chondroitin sulfate chain length and sulfation pattern are essential to cartilage growth activity. Accordingly, a broad spectrum of skeletal dysplasias results from mutations causing undersulfation of chondroitin sulfate chains in humans and in mice[2,7–11]. However, the full impact of defective chondroitin sulfate chain length remains unclear, primarily owing to the lack of a mammalian model.

The SLC35 gene family contains at least 17 human genes that encode NSTs[12]. NSTs are multiple-pass membrane-spanning proteins that transport nucleotide-sugars from the cytosol into the lumens of various organelles. Several NSTs are important in glycosaminoglycan synthesis, supplying specific glycosaminoglycans with substrates for biosynthesis[12]. SLC35D1 transports UDP-GlcUA and UDP-GalNAc, which are substrates for the synthesis of chondroitin sulfate disaccharide repeats[4,5]. This transporter activity suggests that SLC35D1 is involved in chondroitin sulfate biosynthesis; however, much remains to be learned about the biological role of SLC35D1 in chondroitin sulfate biosynthesis.

[1]Laboratory for Developmental Genetics, RIKEN Research Center for Allergy and Immunology, 1-7-22 Suehirocho, Tsurumi-ku, Yokohama, Kanagawa 230-0045, Japan. [2]Laboratory of Bone and Joint Diseases, Single Nucleotide Polymorphism Research Center, RIKEN, 4-6-1 Shirokanedai, Minato-ku, Tokyo 108-8639, Japan. [3]Department of Radiology, Tokyo Metropolitan Kiyose Children's Hospital, 1-3-1 Umezono, Kiyose 204-8567, Japan. [4]Maxillofacial Anatomy, Department of Maxillofacial Biology, and [5]Biochemistry, Department of Hard Tissue Engineering, Division of Biomatrix, Graduate School, Tokyo Medical and Dental University, 1-5-45 Yushima, Bunkyo-ku, Tokyo 113-8549, Japan. [6]Medical Genetics Institute, Cedars-Sinai Medical Center, SSB-3, 8700 Beverly Blvd., and Departments of Human Genetics and Pediatrics, David Geffen School of Medicine at UCLA, Los Angeles, California 90048, USA. [7]Centre for Paediatrics and Adolescent Medicine, Freiburg University Hospital, Mathildenstrasse 1, D-79106 Freiburg, Germany. [8]Department of Pathology, H04.312 University Medical Center Utrecht Postbox 85500, 3508 GA Utrecht, The Netherlands. [9]Faculty of Pharmaceutical Sciences, Chiba University, 1-33, Yayoi, Inage, Chiba 263-8522, Japan. [10]Core Research for Evolutional Science and Technology and [11]Precursory Research for Embryonic Science and Technology, Japan Science and Technology Agency, 4-1-8 Honcho, Kawaguchi, Saitama 332-0012, Japan. [12]Department of Biochemical Cell Research, Tokyo Metropolitan Institute of Medical Science, 3-18-22 Honkomagome, Bunkyo-ku, Tokyo 113-8613, Japan. [13]These authors contributed equally to this work. Correspondence should be addressed to H.K. (koseki@rcai.riken.jp) or S.I. (sikegawa@ims.u-tokyo.ac.jp).

Received 30 April; accepted 21 August; published online 21 October 2007; doi:10.1038/nm1655

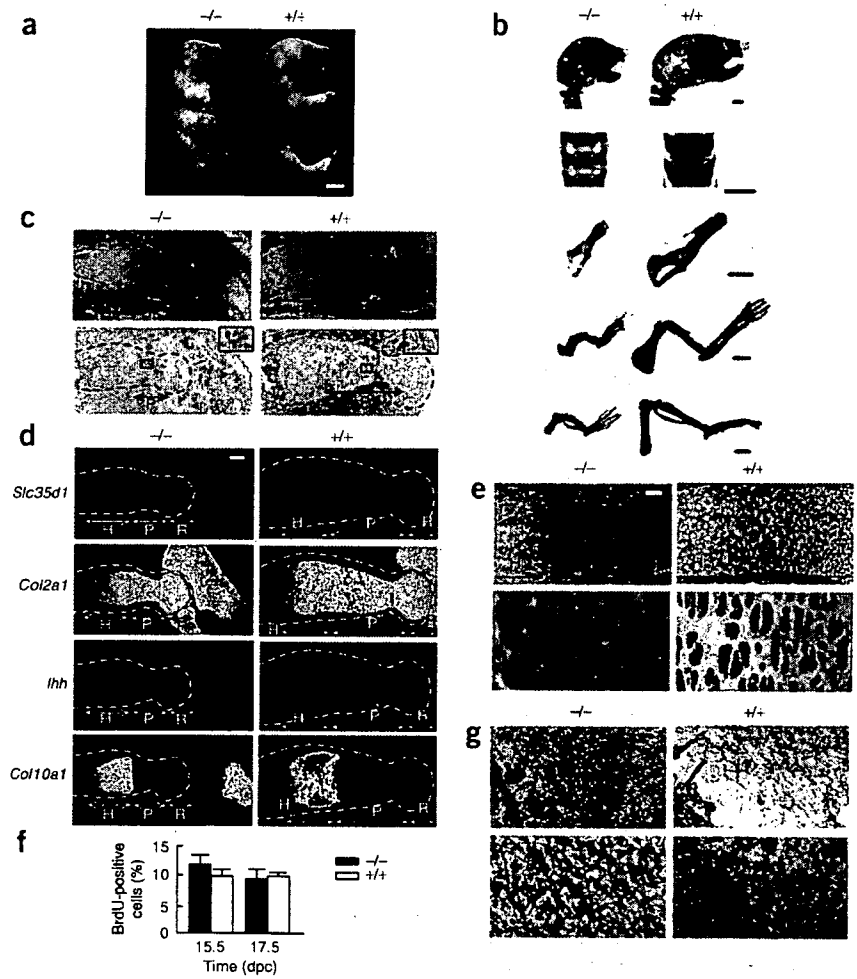

Figure 1 Phenotype of the *Slc35d1*-deficient mice. (**a**) Gross morphology of wild-type (+/+) and *Slc35d1*$^{-/-}$ (-/-) mice at newborn stage. Scale bar, 5 mm. (**b**) Skeletal preparations of 18.5-dpc embryos stained with Alcian blue and Alizarin red. From the top, skull, lumbar spine, ilium, forelimb and hindlimb are shown. Scale bars, 1 mm. (**c–g**) Histological analysis of the epiphyseal cartilage of wild-type and *Slc35d1*$^{-/-}$ embryos. Dashed lines define the humerus. Resting (R), proliferating (P) and hypertrophic (H) zones in the epiphyseal cartilage are demarcated. (**c**) Definition of the proliferating zone by BrdU incorporation. H&E staining (top) and immunostaining with antibody to BrdU (bottom) of the epiphyseal cartilage from BrdU-labeled embryos at 15.5 dpc. Insets at upper right of the lower panels show BrdU-positive cells in the boxed regions. Scale bar, 200 μm. (**d**) *In situ* hybridization to determine the expression of *Slc35d1* and zone-specific molecular marker mRNA in the epiphyseal cartilage of 15.5 dpc embryos. In wild-type cartilage, *Slc35d1* was preferentially expressed in proliferating zones. *Ihh* and *Col10a1* were expressed in prehypertrophic and hypertrophic zones, respectively, whereas *Col2a1* was preferentially expressed in resting and proliferating zones. Expression patterns of the zonal markers were not markedly affected in *Slc35d1*$^{-/-}$ mice. Scale bar, 200 μm. (**e**) H&E staining of the epiphyseal cartilage of 15.5-dpc embryos (top) and toluidine blue staining of plastic sections of the proliferating zone of the epiphyseal cartilage from 15.5-dpc embryos (bottom). Scale bars, 100 μm (top) and 10 μm (bottom). (**f**) Frequency of BrdU-positive cells in the proliferating zone of the epiphyseal cartilage of embryos at 15.5 and 17.5 dpc. The number of BrdU-positive cells and the total number of cells in five sections are from two mice. Values represent mean ± s.e.m. (**g**) Electron microscopic images of ECM from the proliferating zone of the epiphyseal cartilage of 17.5-dpc embryos magnified 10,000× (top) and 300,000× (bottom). A chondrocyte was observed in the lower left corner of the top micrograph. Scale bars, 1 μm (top) and 0.1 μm (bottom).

To clarify the biological role of SLC35D1, we isolated a full-length mouse *Slc35d1* messenger RNA and synthesized its complementary DNA. Its deduced amino acid sequence was 97% identical to that of human SLC35D1. The mouse Slc35d1 protein had substrate specificity and subcellular localization identical to those of its human counterpart (**Supplementary Fig. 1** online). Then we established an *Slc35d1*$^{+/-}$ mouse line that transmits the mutation through the germline (**Supplementary Fig. 2** online). These heterozygous mice showed no phenotypic abnormalities. RT-PCR analysis confirmed the absence of *Slc35d1* transcripts in homozygous embryos. *Slc35d1*$^{-/-}$ mice did not survive the neonatal period; their crown-rump length was reduced and their limbs were extremely short (**Fig. 1a**). Other external phenotypic traits included a short snout, protruding tongue, narrow thorax and protruding abdomen. Skeletal preparations showed hypoplasia of craniofacial bones, flattening of vertebral bodies, longitudinally short ilia and extremely short long bones (**Fig. 1b**). This severe chondrodysplasia confirms that Slc35d1 is crucial during prenatal skeletal development in mice.

To understand the pathogenic basis of the chondrodysplasia phenotype, we investigated the histology of the epiphyseal cartilage of *Slc35d1*$^{-/-}$ mice at 15.5 days post coitus (dpc). Consistent with the shortened limb length, the proliferating zone, as defined by BrdU incorporation, was greatly reduced (**Fig. 1c**). *Slc35d1* expression was intense in the proliferating zone of wild-type but absent in mutant mice (**Fig. 1d**). The *Slc35d1*$^{-/-}$ epiphyseal cartilage showed a disorganized proliferating zone in which the normal columnar alignment of chondrocytes was replaced by closely packed, round chondrocytes and very little extracellular matrix (ECM) space (**Fig. 1e**). The frequency of BrdU-positive cells in the proliferating zone of the mutant mice was similar to that in the wild-type mice (**Fig. 1f**), and TUNEL-positive cells were rarely observed in the proliferating zones of both mutant and wild-type mice (data not shown). The expression patterns of the zone-specific markers *Col2a1*, *Ihh* and *Col10a1* in *Slc35d1*$^{-/-}$ mice were similar to those in wild-type mice (**Fig. 1d**), indicating that the pattern of chondrocyte differentiation was not affected. Electron microscopic analysis of the ECM from the proliferating zones of *Slc35d1*$^{-/-}$ mice showed a loss of the pericellular halo and a denser collagen fibril network (**Fig. 1g**). Higher-magnification images revealed a severe reduction in and amorphous appearance of proteoglycan aggregates (**Fig. 1g**). These findings suggest that proteoglycan synthesis is impaired in *Slc35d1*$^{-/-}$ epiphyseal cartilage.

To characterize abnormal proteoglycan metabolism in the mutant, we examined the distribution of the core protein of aggrecan, a major component of cartilage proteoglycan, and the chondroitin sulfate and

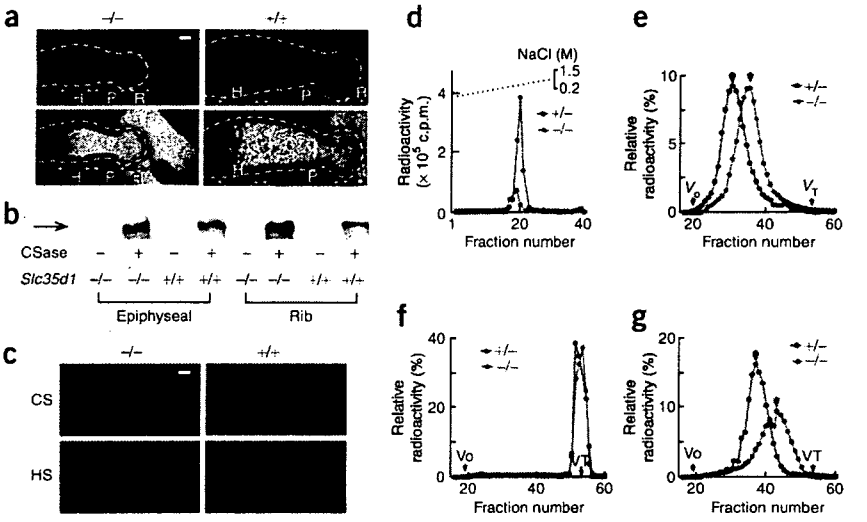

Figure 2 Effects of impaired chondroitin sulfate synthesis on cartilage proteoglycan in *Slc35d1*-deficient mice. (**a**) Immunostaining and *in situ* hybridization analysis for the core protein of aggrecan. Sections from the distal humerus of wild-type (+/+) and *Slc35d1*$^{-/-}$ (-/-) embryos at 15.5 dpc are shown. Dashed lines define the humerus. Zones are indicated as in **Figure 1**. Scale bar, 200 μm. Staining with an antibody to an aggrecan core protein (top) and *in situ* hybridization for the expression of *Agc1* mRNA (bottom) are shown. (**b**) Western blot for aggrecan core protein in the epiphyseal and rib cartilages of 17.5-dpc embryos. The intact aggrecan core polypeptide, with a molecular mass of ~220 kDa (arrow), is visible only after chondroitinase (CSase) treatment in wild-type and homozygote cartilage. (**c**) Staining with antibodies to chondroitin mimotope (CS, top) and heparan sulfate (HS, bottom). Sections from the proliferating zone of the epiphyseal cartilage of 15.5-dpc embryos are used. Scale bar, 10 μm. (**d–g**) Glycosaminoglycan synthesis in cartilage explants. Glycosaminoglycans of proteoglycans in rib-cartilage explants were metabolically labeled with [^{35}S]sulfate for subsequent chromatographic analysis. Open and closed circles indicate samples from *Slc35d1*$^{+/-}$ and *Slc35d1*$^{-/-}$, respectively. Radioactivity is indicated as absolute (**d**) and as relative value (%) as compared to the total analyzed sample (**e–g**). (**d**) Purification of the proteoglycan fraction. Explant extracts were fractionated by Q-Sepharose chromatography and peak fractions were pooled (proteoglycan fraction). Aliquots were used for the following chromatography experiments. (**e**) Sephacryl S-500HR chromatography with untreated samples. The peak positions of *Slc35d1*$^{-/-}$ and *Slc35d1*$^{+/-}$ (arrows) corresponded to dextran of 3.1 × 10^5 kDa and 1.2 × 10^6 kDa, respectively. V_o, exclusion volume of the column; V_t, total volume of the column. (**f**) Superose6 chromatography with samples digested with chondroitinase ABC. (**g**) Superose6 chromatography for glycosaminoglycan analysis. Before loading, the glycosaminoglycans were released from the proteoglycan core proteins by β-elimination. The peak positions of *Slc35d1*$^{-/-}$ and *Slc35d1*$^{+/-}$ (arrows) corresponded to chondroitin sulfate chains of 1.3 × 10^4 kDa and 2.7 × 10^4 kDa, respectively.

heparan sulfate contents in epiphyseal cartilage. Immunostaining and *in situ* hybridization analysis revealed that the amount of aggrecan core did not differ between *Slc35d1*$^{-/-}$ and wild-type mice (**Fig. 2a**). These results were further confirmed by western blot analysis (**Fig. 2b**). Immunohistological studies of chondroitin sulfate and heparan sulfate distribution suggested that the chondroitin sulfate content of the *Slc35d1*$^{-/-}$ epiphyseal cartilage was markedly reduced, whereas the heparan sulfate content was unaltered (**Fig. 2c**). Disaccharide compositional analysis[13] also showed that chondroitin sulfate abundance in the *Slc35d1*$^{-/-}$ cartilage at 18.5 dpc decreased to one-seventh that of the wild type, but heparan sulfate abundance did not change (**Supplementary Table 1** online). These results suggest that the *Slc35d1* mutation causes defects in the chondroitin sulfate biosynthesis of cartilage proteoglycan core proteins.

We further investigated the effects of altered chondroitin sulfate biosynthesis on proteoglycans in *Slc35d1*$^{-/-}$ embryos by labeling newly synthesized chondroitin sulfate with [^{35}S]sulfate in explant cultures of rib cartilage[14]. The radioactivity of the proteoglycan fraction per explant weight in *Slc35d1*$^{-/-}$ mice was reduced to one-third of that in heterozygotic mice, as determined by ion-exchange chromatography (**Fig. 2d**). We next examined the relative molecular mass of proteoglycans by using gel-filtration chromatography. The peak radioactivity in the homozygous mouse extract shifted five fractions toward the total volume of the column (V_T) relative to the heterozygous mouse extract peak. This shift represents a 75% decrease in the average proteoglycan molecular mass in *Slc35d1*$^{-/-}$ extracts (**Fig. 2e**). We confirmed that these radioactive peaks represent chondroitin sulfate by digesting the extract with chondroitinase ABC, which shifted the peaks completely to the V_T (**Fig. 2f**). Finally, we measured chondroitin sulfate chain length by releasing chondroitin sulfate chains from proteoglycan core proteins through β-elimination. In *Slc35d1*$^{-/-}$ extracts, the major radioactive peak was broad, split and shifted to a lower-molecular-mass position (**Fig. 2g**), indicating a reduction in *Slc35d1*$^{-/-}$ cartilage chondroitin sulfate chain length to half of that of the heterozygote. These results indicate that chondroitin sulfate biosynthesis is impaired in *Slc35d1*$^{-/-}$ cartilage.

Schneckenbecken dysplasia (OMIM 269250) is a perinatally lethal skeletal dysplasia that is inherited as an autosomal recessive trait[15–17]. The German term 'Schneckenbecken' refers to the distinctive, snail-like appearance of the ilia that results from a medial bone projection from the inner iliac margin. Other hallmarks of Schneckenbecken dysplasia include thoracic hypoplasia, severe flattening of the vertebral bodies and short, thick long bones. The similarities of the skeletal and histological findings in *Slc35d1*$^{-/-}$ mice to the Schneckenbecken dysplasia phenotype prompted us to search for *SLC35D1* mutations in individuals with Schneckenbecken dysplasia (**Supplementary Table 2** online). In two subjects with typical Schneckenbecken dysplasia (**Supplementary Case Report** online), we found mutations in both alleles (**Fig. 3a**). Subject 1, the product of a consanguineous marriage, was homozygous for a 1–base pair deletion (c.125delA) in exon 1 that produced a premature stop codon (p.S42fsX9). Subject 2 was compound heterozygous for a nonsense mutation in exon 11, c.932G→A (p.W311X) and a splice–donor site mutation, IVS7+1G→T. Sequencing of the RT-PCR product derived from Subject 2 revealed that the IVS7+1G→T mutation causes abnormal splicing, which produces a premature stop codon (**Fig. 3b**). The predicted truncated protein (p.K212insLSSNLKLX) lacks the C-terminal 143 amino acids of SLC35D1 and contains 7 substituted amino acids. Thus, all three mutations are predicted to produce truncated proteins.

Next, we evaluated the NST activity of the predicted SLC35D1 truncation proteins in Subject 2 by using a yeast complementation assay[4,5]. Western blot analysis confirmed the expression of the mutant and wild-type SLC35D1 in microsome fractions prepared from transfected yeast cells (**Fig. 3c**). Although SLC35D1-expressing microsomes

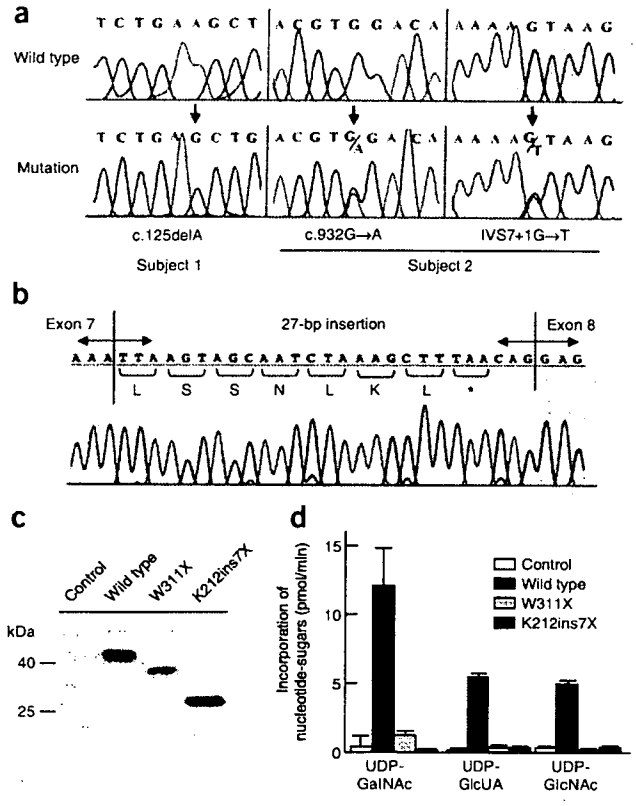

Figure 3 Loss-of-function mutations of *SLC35D1* in Schneckenbecken dysplasia. (**a**) Identification of *SLC35D1* mutations in two patients with typical Schneckenbecken dysplasia. Top schematic shows wild-type sequence and lower schematic mutant sequence. Mutations are indicated by arrows. These mutations were not found in more than 40 ethnicity-matched controls or in public sequence-variation databases. (**b**) Abnormal RNA splicing caused by the IVS7+1G→T mutation in Subject 2. Sequencing of the RT-PCR product encompassing exons 5–9 of RNA from Subject 2 showed an in-frame insertion of 27 nucleotides between exons 7 and 8 (c.636_637 ins27), which produced a premature stop codon. (**c,d**) Loss of nucleotide-sugar transporter activity by mutant SLC35D1 proteins. Microsomes were prepared from yeast cells transfected with empty vector, SLC35D1 or its mutant expression vector. (**c**) Western blots for wild-type and mutant SLC35D1 proteins in yeast microsomes. (**d**) Transporter activities of the mutant SLC35D1 proteins. The incorporation of nucleotide-sugars for 1 min at 30 °C per mg microsome protein is shown. Each value represents the mean ± s.d. of duplicate experiments.

showed higher incorporation of UDP-GalNAc, UDP-GlcUA and UDP-GlcNAc relative to a non-expressing control, those expressing either truncated protein showed the same incorporation levels as the control (**Fig. 3d**). Therefore, both mutant proteins in Subject 2 completely lack NST activity; judging from the considerably shorter length of p.S42fsX9 in Subject 1 (**Supplementary Fig. 3** online), this mutant should also lose activity. These findings indicate that Schneckenbecken dysplasia can be caused by loss of SLC35D1 function.

Thus, we have shown that SLC35D1 has an indispensable role in mouse and human skeletal formation. SLC35D1 deficiency causes the shortening of chondroitin sulfate chains, leading to the disorganization of a functional ECM in epiphyseal cartilage and to skeletal dysplasias. SLC35D1 is a crucial molecule that regulates the chondroitin sulfate length in cartilage proteoglycan by supplying the nucleotide-sugars used as substrates for chondroitin sulfate biosynthesis. Notably, the reduction in the average molecular mass of proteoglycan in the *Slc35d1*$^{-/-}$ cartilage was discordant with that of chondroitin sulfate, as determined by gel-filtration chromatography (**Fig. 2e,g**). These results suggest that not only is the chain length reduced, but so is the number of chondroitin sulfate chains on the aggrecan core in *Slc35d1*$^{-/-}$ mice. SLC35D1 may be involved in both the initiation and the elongation of chondroitin sulfate chain synthesis. Further studies are required to evaluate this possibility.

Our identification of the *SLC35D1* mutation in Schneckenbecken dysplasia contributes to the molecular classification and diagnosis of perinatally lethal skeletal dysplasias. Human skeletal dysplasias are grouped by their phenotypic similarities, which reflect causal similarity in many cases[18]. Schneckenbecken dysplasia belongs to the 'severe spondylodysplastic dysplasias' group, for which no causative mutations were known before this study. *SLC35D1* and other genes acting in the same genetic pathway may well be responsible for these lethal skeletal dysplasias. Also, our findings underscore other NSTs as new candidates for human skeletal dysplasias. Indeed, a missense mutation in the bovine *Slc35a3* gene, which encodes a UDP-GlcNAc transporter, is known to be responsible for complex vertebral malformations[19]. Our study may help build new bridges between skeletal biology and glycobiology.

METHODS

Generation of *Slc35d1*-deficient mice. We generated a knockout mouse line of the *Slc35d1* gene by using methods previously described[20]. A bacterial artificial chromosome (BAC) clone containing the mouse *Slc35d1* was screened from an embryonic stem (ES) cell–BAC library (see Acknowledgments). Using the BAC, we constructed a targeting vector to eliminate the genomic region encompassing exons 1–3 (**Supplementary Fig. 2**). We introduced this vector into R1 ES cells and cloned homologous recombinants through selection with antibiotics and verification of the genotype. We developed chimeric mice with the targeted ES-cell clones and obtained homozygous mice by interbreeding the offspring. All procedures, including mouse handling, were conducted according to guidelines approved by the RIKEN Institutional Animal Care and Use Committee.

Skeletal histology, *in situ* hybridization and immunohistological analysis. We stained bone and cartilage from 18.5 dpc embryos with Alizarin red and Alcian blue as described previously[21]. We prepared paraffin sections (5 μm) processed from 15.5 dpc embryos for H&E staining, *in situ* hybridization and immunohistochemistry. We performed *in situ* hybridizations as previously described[22], using radiolabeled antisense RNA for *Slc35d1*, *Col2a1*, *Ihh*, *Col10a1* and *Agc1*. We performed immunohistological detection of aggrecan core protein and chondroitin mimotope as described elsewhere[23], using specimens pretreated with chondroitinase ABC. We immunodetected heparan sulfate with a heparan sulfate–specific antibody, 10E4 (Seikagaku Corporation). We labeled proliferating cells in 15.5- and 17.5-dpc embryos with BrdU (Sigma-Aldrich Japan) and immunodetected them with antibody to BrdU (clone B44; Nippon Becton Dickinson) as described previously[24].

Transmission electron microscopy. For ultrastructural analysis, we fixed specimens of epiphyseal cartilage taken from the humerus of 17.5-dpc embryos through a 1-d immersion in a 5% (w/v) glutaraldehyde and 4% (w/v) paraformaldehyde solution and a subsequent 3-h soak in 1% (w/v) osmium tetroxide. We embedded specimens in Epon 812 (TAAB) and examined ultrathin sections with the HITACHI H-800 transmission electron microscope (Hitachi).

Western blot analysis. We extracted cartilage protein from 17.5-dpc embryos with 4 M guanidine hydrochloride. We exchanged the guanidine hydrochloride in the extracts to 8 M urea and 0.5% polyoxyethylene(10) lauryl ether, and then removed the urea by dialysis. Subsequently, we digested the samples, equivalent to 5 μg of protein, with 0.01 unit of chondroitinase ABC (Seikagaku Corporation) and analyzed by western blotting with antibodies to the aggrecan core peptide (CHEMICON International).